Open Research Online

The Open University's repository of research publications and other research outputs

The analysis of a mouse model of Lysosomal Storage Disorder uncovers a role for astrocyte dysfunction in neurodegeneration

Thesis

oro.open.ac.uk

The analysis of a mouse model of Lysosomal Storage Disorder uncovers a role for astrocyte dysfunction in neurodegeneration

Chiara Di Malta

Discipline: Life and Biomolecular Sciences

Affiliated Research Center: Telethon Institute of Genetics and Medicine

Thesis submitted in accordance with the requirements of the Open University for the degree of Doctor of Philosophy

May 2012

Date of Submission: 18 May 2012

Date of Award: 4 September 2012

To my mother, my angel

Abstract

Astrocytes are the most abundant cellular population in the brain and their role in neurodegenerative processes is becoming increasingly appreciated. In my PhD project, I investigated the contribution of astrocytes to neurodegeneration in Multiple Sulfatase Deficiency (MSD), a severe Lysosomal Storage Disorder (LSD) caused by mutations in the *Sulfatase Modifying Factor 1 (SUMF1)* gene. Using Cre/Lox mouse models, I found that astrocyte-specific deletion of *Sumf1 in vivo* induced severe lysosomal storage and autophagy dysfunction with consequential cytoplasmic accumulation of toxic substrates. Lysosomal storage in astrocytes was sufficient to induce degeneration of cortical neurons *in vivo*, whereas other neuronal populations were spared. Furthermore, in an *ex vivo* co-culture assay, I observed that *Sumf1*$^{-/-}$ astrocytes failed to support the survival and function of wild type cortical neurons, suggesting a non-cell autonomous mechanism for neurodegeneration in LSDs. Compared to the astrocyte-specific deletion of *Sumf1*, the concomitant deletion of *Sumf1* in both neurons and glia *in vivo* induced a widespread neuronal loss and robust neuroinflammation. Finally, behavioural analysis of mice with astrocyte-specific deletion of *Sumf1* compared to mice with

Sumf1 deletion in both astrocytes and neurons allowed me to link a subset of neurological manifestations of LSDs to astrocyte dysfunction. This study indicates that astrocytes are integral components of the neuropathology in LSDs and that modulation of astrocyte function may impact the disease course.

Table of contents

Abstract

List of figures and tables

Abbreviations

4-MU   4-methylumbelliferone

ADP adenosine diphosphate

ALR autophagic lysosome reformation

ALS Amyotrophic lateral sclerosis

ANLS   astrocyte-neuron lactate shuttle

ARSA   *Arylsulfatase A*

ARSB   *Arylsulfatase B*

ARSC   *Arylsulfatase C*

ARSE   *Arylsulfatase E*

ATP adenosine triphosphate

AVs autophagosomes

BAC bacterial artificial chromosome

bp base pairs

BSA bovine serum albumin

CA carbonic anydrase

cDNA complementary DNA

CDPX1 Chondrodysplasia punctata 1

CKO Conditional knockout

CNS central nervous system

CysGly cysteinylglycine

DAMP danger associated molecular pattern

DMEM/F12 Dulbecco's modified Eagle medium: Nutrient Mixture F-12

E15.5 embryonic day 15.5

EAAC Excitatory amino-acid carrier

EAAT Excitatory amino-acid transporter

ER endoplasmic reticulum

EST expressed sequence tag

EYFP enhanced yellow fluorescent protein

FBS fetal bovine serum

FGE Formylglycine-generating enzyme

FGly formylglycine

flox LoxP-flanked

FLP flippase

FRT FLP recognition target

GAG glycosaminoglycan

GFAP   glial fibrillary acidic protein

GFP green fluorescent protein

GLAST (human EAAT1)   Glutamate–aspartate transporter

GLT-1 (human EAAT2)   Glial glutamate transporter 1

Glut glutamate

GLUT1   glucose transporter 1

GLUL   Glutamate-ammonia ligase

GSH glutathione

GGT Gamma-glutamyl transpeptidase

HS horse serum

HSCT   hematopoietic stem cell transplantation

KO Knockout

MAP1LC3A **(abbreviated LC3)** Microtubule-associated proteins 1A/1B light chain 3A

LSD Lysosomal Storage Disorder

MAP-2 Microtubule-associated protein-2

MCT monocarboxylate transporter

MECP2 *methyl CpG binding protein 2*

MEM minimum essential medium

MLD Metachromatic Leukodystrophy

MPS Mucopolysaccharidosis

MSD Multiple Sulfatase Deficiency

NBC Na+/HCO3- Cotransporter

Neo neomycin

NeuN neuronal nuclear protein

NHE sodium-hydrogen exchange

NMDA N-Methyl-D-aspartate

Npc1 *Niemann-Pick disease, type C 1*

NPCs neural precursor cells

NS not stimulated

OCT optimum embedding temperature compound

PBS phosphate buffered saline

PCR polymerase chain reaction

PFA paraformaldehyde

ROS reactive oxygen species

RT room temperature

***SQSTM1* (also known as p62)** *Sequestosome 1*

STS Steroid sulfatase

SUMF1 *Sulfatase Modifying Factor 1*

TCA tricarboxylic acid

TLR Toll-like receptors

VDCC Voltage-dependent calcium channels

WT Wild type

XLI X-linked ichthyosis

Introduction

1.1 Sulfatases and human diseases

Sulfatases are a family of enzymes that catalyze the hydrolysis of sulfate ester bonds, such as O-sulfates and N-sulfates, from a wide variety of substrates, ranging from complex molecules, such as glycosaminoglycans, to sulfolipids and steroid sulfates. The general reactions catalized by sulfatases are:

$$R\text{-}OSO_3^- + H_2O \rightarrow R\text{-}OH + H^+ + SO_4^{2-}$$

$$R\text{-}NHSO_3^- + H_2O \rightarrow R\text{-}NH_3^+ + SO_4^{2-}$$
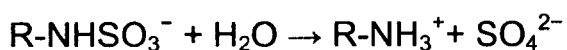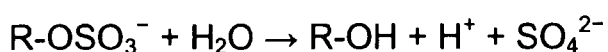
Sulfatases are found in most species from bacteria to eukaryotes and share the following features: (*a*) they have a similar size, ranging from 500 to 800 amino acids, (*b*) they are extensively glycosylated, (*c*) they share significant sequence homology over their entire length, and in particular in the N-terminal region, and (*d*) they have a highly similar active site, which undergoes a unique posttranslational modification (Sardiello et al., 2005).

Figure 1.1 shows the sequence alignment of all 17 human sulfatases in three regions, which represent highly conserved protein domains (domains a, b, and c).

a

ARSC	PNIILVMADDLGIGDPG	43
ARSD	PNILLINADDLGTGDLG	57
ARSH	PNIVLLNADDLGVGDLC	23
ARSE	PNILLLNADDLGIGDIG	54
ARSF	PNIVLINVDDLGIGDLG	47
ARSG	PNFVIILADDMGWGDLG	52
ARSA	PNIVLIFADDLGYGDLG	37
GALNS	PNILLLLMDDMGWGDLG	47
ARSB	PHLVFLLADDLGWNDVG	61
ARSJ	PHLIFILADDQGFRDVG	92
ARSI	PHIIFILTDDQGYHDVG	63
SGSH	RNALLLLADDGGFESGA	39
GNS	PNVVLLLTDDQDEVLGG	63
SULF1	PNIILVPTDDQDVELGS	59
SULF2	PNIILVLTDDQDVELGS	60
TSULF	PNVVLVVSDSFDGRLTF	48
IDS	LNVLLIIVDDLRPSLGC	53

b

ARSC	ASPLCTPSRAAFMTGRYPV	89
ARSD	AAPLCTPSRAAFLTGRHSF	103
ARSH	AASMCTPSRAAFLTGRYPI	69
ARSE	AASLCTPSRAAFLTGRYPV	100
ARSF	AASLCSPSRSAFLTGRYPI	93
ARSG	AASTCSPSRASLLTGRLGL	98
ARSA	PVSLCTPSRAALLTGRLPV	83
GALNS	ANPLCSPSRAALLTGRLPI	93
ARSB	TQPLCTPSRSQLLTGRYQI	105
ARSJ	VQPICTPSRSQFITGKYQI	136
ARSI	IQPICTPSRSQLLTGRYQI	107
SGSH	SVSSCSPSRASLLTGLPQH	84
GNS	PSALCCPSRASILTGKYPH	105
SULF1	TTPMCCPSRSSMLTGKYVH	101
SULF2	TTPMCCPSRSSILTGKYVH	102
TSULF	NSPICCPSRAAMWSGLFTH	94
IDS	QQAVCAPSRVSFLTGRRPD	98

c

ARSC	KDQGYSTALIGKWHLGMS	140
ARSD	QQHGYATGLIGKWHQGVN	154
ARSH	QHRGYRTGLIGKWHLGLS	121
ARSE	KEKGYATGLIGKWHLGLN	151
ARSF	KKQGYSTGLIGKWHQGLN	144
ARSG	QQAGYVTGIIGKWHLGHH	143
ARSA	AARGYLTGNAGKWHLGVG	129
GALNS	KKAGYVSKIVGKWHLGHR	146
ARSB	KEAGYTTHNVGKWHLGMY	151
ARSJ	KEVGYSTHNVGKWHLGFY	182
ARSI	QEAGYSTHNVGKWHLGFY	153
SGSH	SQAGVRTGIIGKKHVGPE	129
GNS	SNCGYQTFFAGKYLNEYG	155
SULF1	NNTGYRTAFFGKYLNEYN	148
SULF2	NSTGYRTAFFGKYLNEYN	149
TSULF	ERHGYRTQKFGKLDYTSG	134
IDS	KENGYVTMSVGKVFHPGI	141

Figure 1.1: Sequence alignment of conserved domains among human sulfatases. (a) and (c) represent domains from the N-terminal of the proteins. (b) represents the active site. Shaded amino acids are conserved in 90% of all sulfatases. The asterisks mark the amino acids with a known catalytic function. Reproduced from (Diez-Roux and Ballabio, 2005)

3

Sulfatases present different substrate specificities and can be divided, at least in mammals, into two main categories based on their subcellular localization: those acting at an acidic pH, localized in the lysosomes, and those acting at a neutral pH that are found in the endoplasmic reticulum (ER), in the Golgi apparatus, and at the cell surface (Table 1.1). The lysosomal sulfatases are involved in catabolic cellular functions, whereas the functions of the non-lysosomal sulfatases is less clear (Parenti et al., 1997; Hanson et al., 2004; Diez-Roux and Ballabio, 2005). The only sulfatase in this category whose metabolic role has been thoroughly characterized is the steroid sulfatase (STS/ARSC), which is involved in the biosynthesis of several steroid molecules (Ballabio A, 2001).

In addition SULF1 and SULF2, two newly identified sulfatases, are located on the cell surface where exert the desulfation of extracellular heparan sulfate proteoglycan, whose sulfation state influences the binding of signaling molecules to their receptor (Bulow and Hobert, 2006). Furthermore the expression of these sulfatases is developmentally regulated, therefore, they specify a novel functional category within the sulfatase family that is involved in cell signaling and embryonic development (Dhoot et al., 2001).

Mutations in many sulfatase genes are responsible for different human

genetic disorders (Neufeld EF, 2001a; Von Figura K, 2001)(Table 1.1).

Gene	Chromosomal localization	Enzyme	Subcellular localization	Human disorder
ARSA	22q13	Arylsulfatase A	Lysosomal	Metachromatic leukodystrophy (MLD)
ARSB	5q13	Arylsulfatase B	Lysosomal	Maroteaux-Lamy syndrome (MPSVI)
IDS	Xq27-28	Iduronate Sulfatase	Lysosomal	Hunter syndrome (MPSII)
SGSH	17q25.3	Sulfamidase	Lysosomal	Sanfilippo A syndrome (MPSIIIA)
G6S	12q14	Glucosamine-6-Sulfatase	Lysosomal	Sanfilippo D syndrome (MPSIIID)
GAL6S	16q24	Galactose-6-Sulfatase	Lysosomal	Morquio A syndrome (MPSIVA)
ARSC/STS	Xp22.3	Arylsulfatase C/Steroid sulfatase	Microsomal	X-linked Ichthyosis (XLI)
ARSD	Xp22.3	Arylsulfatase D	ER	NI
ARSE	Xp22.3	Arylsulfatase E	Golgi	Chondrodysplasia Punctata 1 (CDPX1)
ARSF	Xp22.3	Arylsulfatase F	ER	NI
ARSHa	Xp22.3	Arylsulfatase H	ND	NI
HSULF1	8q13.2-13.3	Hsulf1	Cell surface	NI
HSULF2	20q13.12	Hsulf2	Cell surface	NI
ARSG	17q23-24	Arylsulfatase G	ER	NI
ARSJb	4q26	Arylsulfatase J	ER	NI
ARSIb	5q32	Arylsulfatase K	ER	NI
TSULFa	5q15	T. Sulfatase	ND	NI

Table 1.1: Main characteristics of human sulfatases. Reproduced from (Diez-Roux and Ballabio, 2005)

1.2. Deficiency of lysosomal sulfatases

In human the deficiency of a given lysosomal sulfatase causes a block in the catabolic pathway involved in the degradation of complex sulfated macromolecules, such as glycosaminoglycans (GAGs) and sulfated glycolipids, with their consequent accumulation in cells and tissues. The phenotypic consequences depend on type and tissue distribution of the accumulating substrate. These diseases belong to the lysosomal storage disorders, a group of genetic diseases characterized by the accumulation of undigested material inside cells and tissues due to lysosomal dysfunction (Cox and Cachon-Gonzalez, 2012). Namely, sulfatase deficiencies are associated to Metachromatic Leukodystrophy (MLD) and to five different types of Mucopolysaccharidoses (MPS II, IIIA, IIID, IVA, and VI) (Table 1.2).

MLD is an autosomal recessive disorder with an estimated frequency of 1 in 40,000 births. MLD is caused by loss-of-function mutations of the *Arylsulfatase A* (*ARSA*) gene that codes for a sulfatase normally deputed to the desulfation of glycolipids, such as sulfatides, inside the lysosome (Von Figura K, 2001). Sulfatides are an important component of the myelin sheath (a fatty layer covering the nerve fibers), produced by oligodendrocytes in the central nervous system and by Schwann cells in the peripheral nervous system (Abe and

Norton, 1974); (Benjamins et al., 1974). Without a functional *ARSA*, sulfatides accumulate in the cytoplasm of oligodendrocytes and Schwann cells causing their dysfunction and, in turn, the progressive de-myelination of nerve fibers. The symptoms of the disease are progressive and include gait disturbance, mental regression, loss of speech, optic atrophy, ataxia, and spastic tetraparesis.

The term Mucopolysaccharidoses (MPS) refers to a group of lysosomal storage disorders caused by deficiency in enzymes catalyzing the stepwise degradation of glycosaminoglycans (GAGs) (formerly called mucopolysaccharides) (Neufeld EF, 2001b). The GAGs represent the sugar moiety of the proteoglycans that are a major component of the extracellular matrix, the "filler" substance existing between cells. Proteoglycans are involved in a wide variety of functions ranging from the binding of cations and water to regulating the movement of molecules. Evidence also shows they can affect the activity and stability of proteins and signalling molecules within the matrix. Individual functions of proteoglycans can be attributed to either the protein core or the attached GAG chain (Bulow and Hobert, 2006).

Glycosaminoglycans are large linear polysaccharides constructed of repeating disaccharide units with the primary configurations containing

an amino sugar (either N-Acetylglucosamine or N-Acetylgalactosamine) and an uronic acid (either glucuronic acid and/or iduronic acid). There are five identified glycosaminoglycan chains: hyaluronan; chondroitin; dermatan; heparin/heparin; keratin. Hyaluronan is not sulfated, but the other glycosaminoglycan chains contain sulfate residues at various positions of the chain. Various degrees of sulfation occur at the oxygen and/or nitrogen containing groups, on each monosaccharide unit (Bulow and Hobert, 2006). GAG desulfation, a necessary step for their degradation, is exerted by sulfatase inside the lysosome.

To date the deficiency of five sulfatases are associated to a specific type of MPS: iduronate sulfatase to MPS II (Hunter syndrome); heparan N-sulfatase to MPS IIIA (Sanfilippo A syndrome); N-acetlyglucosamine 6-sulfatase to MPS IIID (Sanfilippo D syndrome); galactose 6-sulfatase to MPS IVA (Morquio A syndrome); N-acetylgalactosamine 4-sulfatase to MPS VI (Maroteaux-Lamy syndrome) (Neufeld EF, 2001b). All are transmitted in an autosomal recessive manner, except for MPS II, which is X linked.

All MPSs display a complex phenotype with involvement of several tissues and organs, a progressive course of the disease, and a great

variability in the expression of the symptoms. These include, in different combinations, facial dysmorphisms, skeletal deformities, hepatosplenomegaly, joint and skeletal abnormalities, corneal clouding, hearing defects, respiratory and cardiovascular defects, mental retardation, and neurological abnormalities. Profound mental retardation is characteristic of the severe form of Hunter syndrome and all subtypes of Sanfilippo syndrome, which is characterized by severe central nervous system degeneration (Neufeld EF, 2001b) (Table 1.2).

Name	Abbreviation	Inheritance pattern	Enzyme deficiency	Main disease manifestations
Metachromatic leukodystrophy	MLD	Autosomal recessive	Arylsulfatase A	Demyelinization of central and peripheral nervous system
Hunter syndrome	MPSII	X-linked recessive	Iduronate sulfatase	Dysostosis multiplex Organomegaly Mild to severe mental retardation
Sanfilippo A syndrome	MPSIIIA	Autosomal recessive	*Sulfamidase*	Hyperactivity Mild somatic features
Sanfilippo D syndrome	MPSIIID	Autosomal recessive	N-acetlyglucosamine-6-sulfatase	Severe neurological manifestations
Morquio A syndrome	MPSIV	Autosomal recessive	Galactose 6-sulfatase	Severe skeletal abnormalities Corneal clouding
Maroteaux-Lamy syndrome	MPSVI	Autosomal recessive	Arylsulfatase B	Dysostosis multiplex Corneal clouding
X-linked ichthyosis	XLI	X-linked recessive	Arylsulfatase C/Steroid sulfatase deficiency	Dark scaly skin Mild corneal opacities
Chondrodysplasia Punctata 1	CDPX1	X-linked recessive	Arylsulfatase E	Aberrant bone mineralization Nasal hypoplasia Short stature Distal phalangeal hypoplasia

Table 1.2: Diseases due to single sulfatase deficiencies. Reproduced from (Diez-Roux and Ballabio, 2005)

11

1.3 Deficiency of non-lysosomal sulfatases

This category includes two disorders (both X-linked) caused by deficiencies of sulfatases located in cellular compartments other than lysosomes and acting at a neutral rather than an acidic pH.

One of them is the steroid sulfatase (STS). This enzyme is localized primarily in the ER and is involved in the desulfation of steroid sulfates, the reservoir or a source of precursors for producing active hormones. STS deficiency is the biochemical hallmark of an inherited skin disease called X-linked ichthyosis (XLI), whose major feature is the presence of dark scaly skin (Marinkovic-Ilsen et al., 1978) (Table 1.2). Interestingly, babies affected by this disease are usually born by caesarean section due the lack of production of estriol by the placenta caused by STS deficiency, leading to refractoriness to the onset of labor (also described as uterine inertia) (France and Liggins, 1969). Affected babies appear normal at birth, and the placentas lack anatomic defects. Ichthyosis becomes apparent in STS-deficient babies between 0 to 3 months and slightly improves with age. The scales are due to an altered cholesterol sulfate/cholesterol ratio in the stratum corneum of the epidermis (France et al., 1973).

The second disorder due to deficiency of a non-lysosomal sulfatase is Chondrodysplasia punctata 1 (CDPX1), a congenital defect of bone

and cartilage development characterized by aberrant bone mineralization manifested by punctate calcification of bone epiphyses, severe underdevelopment of nasal cartilage, and distal phalangeal hypoplasia (Table 1.2). The gene mutated for CPDX1 is *Arylsulfatase E* (*ARSE*) (Franco et al., 1995). The ARSE protein is located in the Golgi apparatus but its natural substrate has not yet been identified and therefore its metabolic function remains elusive.

1.4 Posttranslational modification of sulfatases and Multiple Sulfatase Deficiency

To be active, sulfatases require a critical post-translational modification that occurs before their targeting to different cellular compartments, consisting of the conversion of a cysteine residue located within their active site into a 2-amino-3-oxopropanoic acid [α-formylglycine (FGly)] (Schmidt et al., 1995). The modified cysteine residue is highly conserved across evolution, and is present in all sulfatases (Sardiello et al., 2005)(Fig 1.1b).

The enzyme responsible for sulfatase activation is known as formylglycine-generating enzyme (FGE) (Cosma et al., 2003) (Dierks et al., 2003). The FGE is located into the ER and it recognizes a short sequence motif, C-[TSAC]-PSR, which is necessary and sufficient for specific FGE–sulfatase interaction within the ER immediately after sulfatase translation (Roeser et al., 2006)

The gene encoding FGE is the *Sulfatase Modifying Factor 1* (*SUMF1*) gene and when mutated it is responsible for a severe form of lysosomal storage disorder known as Multiple Sulfatase Deficiency (MSD) (Cosma et al., 2003) (Dierks et al., 2003) (Cosma et al., 2004; Dierks et al., 2005; Schlotawa et al., 2011). MSD is extremely rare (1:1.4million births), and it is transmitted in an autosomal recessive

manner. At biochemical level, MSD is characterized by a profound impairment of all sulfatase activities that in turn lead to intracellular accumulation of the sulfatase substrates (Figure 1.2). As a consequence, the phenotype of MSD patients combines all the clinical symptoms observed in individual sulfatase deficiencies (Table 1.2) such as ataxia, progressive loss of motor, speech, vision and hearing abilities, hepatosplenomegaly, dysostosis multiplex, abnormal facies, stiff joints, and ichthyosis. The patients usually die within the first decade of life (Hopwood JJ, 2001).
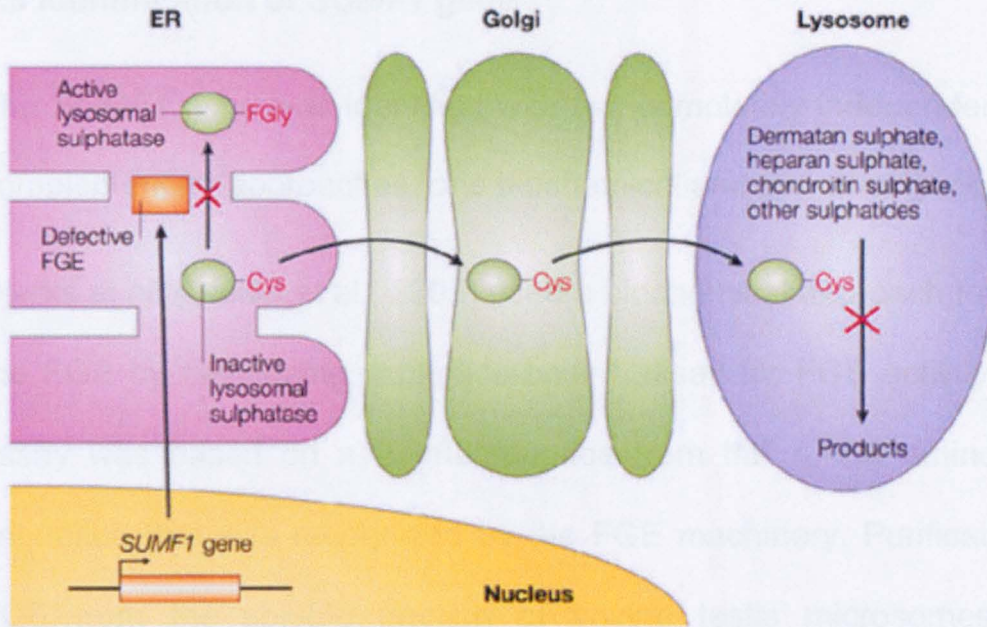
Figure 1.2: **Mutations in the *Sulfatase Modifying Factor-1* (*SUMF1*) gene result in the production of defective α-formylglycine-generating enzyme (FGE).** Defective FGE cannot convert the cysteine (Cys) residue that is found at the active site of lysosomal sulfatases to α-formylglycine (FGly). As a result, inactive sulfatases are transported to the lysosome, where they are unable to degrade various sulfate esters. This leads to sulfate-ester accumulation and subsequently to MSD. ER, endoplasmic reticulum. Reproduced from (Futerman and van Meer, 2004)

1.5 Identification of *SUMF1* gene

The *SUMF1* gene was identified with two completely independent and complementary approaches, one biochemical and the other genetic.

Dierks et al. (Dierks et al., 2003) used a biochemical approach to purify the FGE by developing a peptide-based assay for FGE activity. This assay was based on a 23-mer peptide from the *ARSA* amino acid sequence that was recognized by the FGE machinery. Purification of FGE from the soluble fraction of bovine testis microsomes was performed utilizing a four-step chromatography. The resulting peptides were subjected to peptide mass fingerprint analysis, leading to the amino acid sequence of FGE and to the discovery of the corresponding cDNA in expressed sequence tag (EST) databases. This cDNA was found mutated in patients with MSD.

A genetic complementation approach was used by Cosma et al. (Cosma et al., 2003), who performed microcell-mediated chromosome transfer to identify the gene complementing the enzymatic deficiency in MSD. A panel of human/mouse hybrid lines containing individual normal human chromosomes, tagged with two selectable markers, was the source of donor human chromosomes and was fused to an immortalized cell line from a patient with MSD. All 22 human

autosomes were transferred one by one and the resulting colonies tested for sulfatase enzymatic activity. This analysis allowed the assignment of the gene to chromosome 3. Then, irradiation followed by microcell-mediated chromosome transfer allowed mapping of the complementing gene to a smaller chromosomal region, spanning approximately 2.4Mb. All genes located in this region were tested for mutations in MSD patients until one of them was found mutated in all patients tested.

SUMF1 is both an essential and a limiting factor for the activity of sulfatases (Fig 1.3). In normal condition the amount of SUMF1 is sufficient for the post-translational activation of all sulfatases (Fig 1.3A). In MSD patients the lack of SUMF1 results in inactive sulfatases (Fig 1.3B). Due to a limited availability of SUMF1, the overexpression of a sulfatase only partially increases the sulfatase enzymatic activity despite the amount of protein produced (respectively, smaller circle and larger circle in Fig 1.3C). An increase in a sulfatase enzymatic activity occurs only when this is co-expressed with SUMF1 (large circle in Fig1.3D) (Cosma et al., 2003).
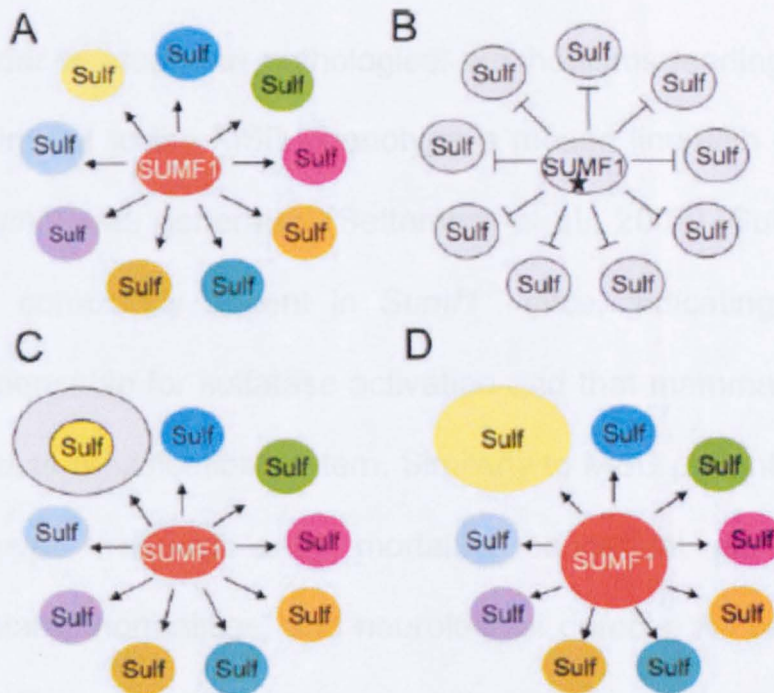
Figure 1.3: *SUMF 1* **is an essential limiting factor for the activity of** **sulfatases.** (A) *SUMF1* activates sulfatases in physiological conditions. (B) If *SUMF1* is mutated, as in MSD, the activity of all sulfatases is impaired. (C) If a sulfatase is overexpressed, the activity is partial (smaller circle) relative to the amount of protein produced (larger circle) due to the limiting amount of *SUMF1* protein. (D) A complete activation of a sulfatase (large circle) only occurs when both the sulfatase and *SUMF1* are overexpressed. Reproduced from (Cosma et al., 2003)

1.6 The MSD mouse model

In order to study the pathological mechanisms leading from sulfatase impairment to the MSD phenotype a mouse line with genetic deletion of *Sumf1* was generated (Settembre et al., 2007). Sulfatase activities were completely absent in *Sumf1*$^{-/-}$ mice, indicating that *Sumf1* is indispensable for sulfatase activation and that mammals have a single sulfatase modification system. Similarly to MSD patients, *Sumf1*$^{-/-}$ mice displayed frequent early mortality, congenital growth retardation, skeletal abnormalities, and neurological defects. All tissues examined showed progressive cell vacuolization and significant lysosomal storage of GAGs. The prominent and progressive neurodegeneration was characterized by remarkable neuronal cell loss associated with activated microglia and astroglyosis throughout the brain.

1.7 Neuropathological mechanisms in MSD

1.7.1 Impaired autophagy

As for many other LSDs, progressive and severe neurodegeneration is a prominent feature of MSD (Platt FM, 2004). Previous studies identified impaired autophagy in neurons as a crucial component in the pathogenic mechanisms leading to neurodegeneration in MSD as well as in other LSDs (Settembre et al., 2008b).

During autophagy a large portion of the cytosol is sequestered in specific vesicles (autophagosomes, AVs) and then degraded upon fusion with lysosomes. Through basal autophagy the cell regulates turnover of organelles, such as mitochondria, peroxisomes and endoplasmic reticulum. Beyond the basal activity, autophagy can be induced as response to many adverse circumstances: during nutrient depletion autophagy allows generation of ATP from the catabolism of macromolecules; during oxidative stress, induction of autophagy allows the efficient removal of damaged organelles and proteins from the cytoplasmatic environment, acting as a pro-survival pathway (Ravikumar et al., 2006).

Lysosomal storage may dampen the last steps of the autophagic process. A defective autophagy in LSDs was proposed to be a consequence of an impaired lysosome-autophagosome fusion. Settembre et al., showed a decreased co-localization of the lysosomal marker LAMP1 with the autophagosomal marker LC3 in MSD mouse embryonic fibroblasts (MEFs) compared with wild-type cells (Settembre et al., 2008b). Fraldi et al., confirmed and extended this observation using a tandem fluorescent-tagged autophagosomal marker in which LC3 was engineered with both the monomeric red-fluorescent protein (mRFP) and the green fluorescent protein (GFP) tags. The quenching of GFP fluorescence into the intra-lysosomal acidic pH allowed to measure the rate of autophagosome fusion with lysosome. This rate was found markedly slower in MSD cells compared with WT cells. The decreased fusion was also confirmed in MEFs isolated from another type of LSD, the MPSIIIA (Fraldi et al., 2010). Furthermore, studies performed on cells isolated from patient affected from a different type of LSD (Mucolipidosis type IV) also demonstrated an impairment of fusion of late endosomes/lysosomes (CD63 signal) with LC3-positive vesicles (Vergarajauregui et al., 2008). Other evidences suggest that in cells affected by LSD the lysosome, upon fusion with autophagosome, cannot degrade the autophagic

content leading to cytosolic accumulation of large autophagolysosomes. One unifying possibility could be that the incomplete autophagic degradation inhibits the autophagic lysosome reformation (ALR) process, through which the cell restores its pool of lysosomes (Yu et al., 2010). This block, in turn, may lead to a lysosomal depletion that slower the fusion efficiency between newly generated autophagosomes and lysosomes.

Indeed, autophagosome accumulation was found in neurons from the mouse model of MSD and other LSDs, associated with the accumulation of autophagy substrates, such as poliubiquitinated proteins and aberrant mitochondria (Settembre et al., 2008b). This evidence suggests that the secondary accumulation of autophagic substrates may have a role in LSD pathogenesis. Many of the proteins that cause late-onset neurodegenerative conditions, such as Huntington's and familial forms of Parkinson's diseases, are autophagy substrates (Rubinsztein, 2006). Thus, autophagy dysfunction represents an important point of intersection between lysosomal storage diseases and more common types of neurodegenerative diseases.

1.7.2. Neuroinflammation

Another point of intersection between lysosomal storage diseases and neurological disorders such as Alzheimer's disease (Tuppo and Arias, 2005), Amyotrophic lateral sclerosis (McGeer and McGeer, 2002), Parkinson's disease (Tansey and Goldberg, 2010) and Prion diseases (Perry et al., 2002) is the mounting of an atypical inflammatory response that is mediated by microglia and astrocytes in the innate immune system. The principal mechanism through which an innate immune response is initiated, involves signalling through the TLR family of receptors (Crack and Bray, 2007). It has become clear that injured cells, including neurons (Sloane et al., 2010), release a class of molecules known as "danger associated molecular pattern" (DAMP) ligands that bind to TLR receptors present on microglia and initiate an innate immune response. Activated microglia may exhibit behaviours associated with anti-inflammatory macrophages, secreting molecules that promote tissue repair and internalizing cellular debris, including aggregated, misfolded proteins, such as b-amyloid, through phagocytosis. Alternatively, responding microglia may adopt a pattern of behaviour similar to pro-inflammatory macrophages as they release molecules intended to protect against pathogens, including neurotoxic

cytokines, reactive oxygen species (ROS), and small molecules, such as quinolinic acid, that promote excitotoxicity (Colton, 2009). The release of cytokines and chemokines can lead to the recruitment of additional inflammatory cells (macrophages) from adjacent blood vessels, and may also engage astrocytes in the proinflammatory response. Activation of astrocytes induces astrogliosis, which is characterized by altered gene expression, hypertrophy, and proliferation (Ridet et al., 1997). Activated astrocytes can release a wide array of immune mediators such as cytokines, chemokines, and growth factors, that may exert either neuroprotective or neurotoxic effects (Farina et al., 2007). In conclusion, neuroinflammatory responses to neuronal dysfunction in neurodegenerative disorders present a complex nature, being potentially beneficial or detrimental depending on the fine balance between a number of factors, including the type, the duration and the severity of the insult and the complex interplay between the various cytokines released by microglia and astrocytes and their receptors.

However, the molecular event triggering microglia and astrocyte activation in lysosomal storage disorders may be more ambiguous. Microglia and astrocytes store undigested material in their cytoplasm

(Settembre et al., 2007); this storage may alter their physiological state, hence trigger their activation and, consequently, drive neuroinflammation.

1.7.3. Proposed model for the pathogensis of LSDs

A possible model for the pathogenesis of MSD and LSDs in general has been proposed (Figure 1.4). According to this model the lysosomal storage leads to a block of the autophagic flux causing a secondary accumulation of autophagy substrates such as polyubiquitinated proteins, p62/SQSTM1 and dysfunctional mitochondria in different cell types, included neurons (Lieberman et al., 2012). The accumulation of these secondary substrates is reported to be toxic for the cell and may contribute to cell death. The inflammatory response to cell damage may further exacerbate the phenotype (Fig 1.4) (Ballabio and Gieselmann, 2009). This model suggests how neuronal cell loss, hence, neurodegeneration, proceeds in MSD. To date, research has focused on neurons, however glia cells are affected by the same genetic defect and impairment of their function may significantly contribute to the neuronal dysfunction observed in MSD.
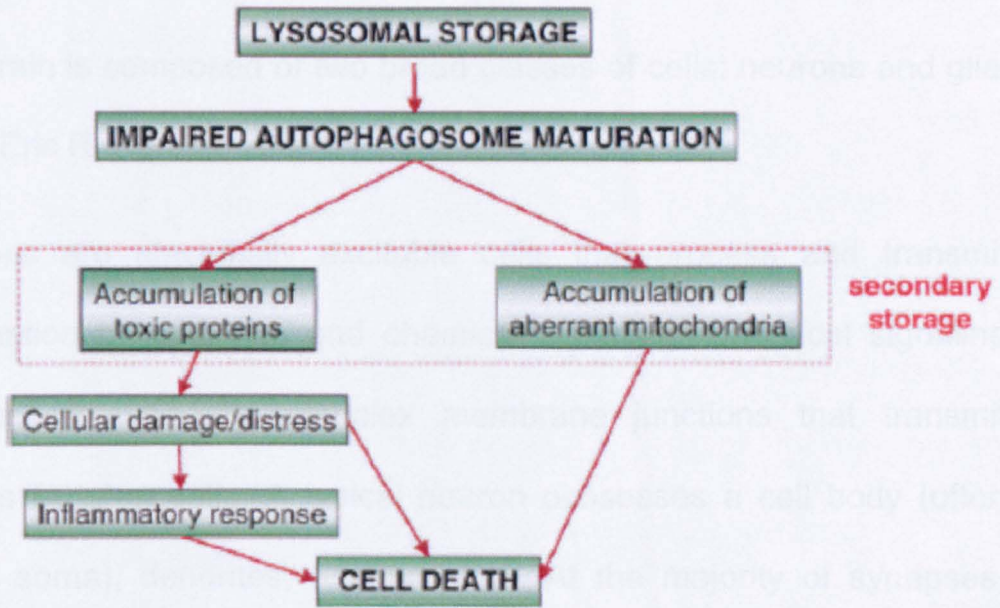
Figure 1.4: A proposed model for the pathogenesis of LSDs. Adapted from (Ballabio and Gieselmann, 2009)

1.8   Brain cell types

The brain is composed of two broad classes of cells: neurons and glial cells (Eric R. Kandel, 2000).

Neurons are electrically excitable cells that process and transmit information by electrical and chemical signaling. Chemical signaling occurs via synapses, complex membrane junctions that transmit signals to other cells. A typical neuron possesses a cell body (often called soma), dendrites, and an axon. At the majority of synapses, signals are sent from the axon of one neuron to a dendrite of another, in this way neurons connect to each other to form neural networks.

Glial cells, sometimes called neuroglia, are the non-neuronal cells of the central nervous system (CNS). The term glia (from the Greek word meaning "glue") reflects the nineteenth-century presumption that these cells held the nervous system together in some way. The word has survived, despite much more complex roles have been recognized to glia.

There are three types of glial cells in the mature central nervous system: astrocytes, oligodendrocytes, and microglial cells.

- Astrocytes main function is to maintain, in a variety of ways, an appropriate chemical environment for neuronal signaling. Because of the interest for this thesis work, the next paragraph is aimed to elucidate astrocyte morphological features and functions.

- Oligodendrocytes lay down a laminated, lipid-rich wrapping called myelin around neuronal axons. This has important effects on the speed of action potential conduction.

- Microglial cells, as the name implies, are the smaller cells among glia, and they derive from hematopoietic stem cells. They share many properties with tissue macrophages, and are primarily scavenger cells that remove cellular debris from sites of injury or normal cell turnover (Eric R. Kandel, 2000).

1.9 Astrocytes

Astrocytes are the most abundant cell type in the mammalian brain. They greatly outnumber neurons, and are organized into discrete subdivisions at the anatomical level, within which as many as 100,000 synapses can be located (Benarroch, 2005). In such regions, astrocytes extend their cell membranes into and among neuronal synapses, forming closely interdigitating areas of direct apposition. In addition, astrocytes project specialized endfeets in close contact with intraparenchymal blood vessels, almost entirely covering their surface (Benarroch, 2005).

These features, ideally position astrocytes to play crucial roles in adult CNS homeostasis, performing a variety of functions reflecting their communication and close interaction with neurons (Belanger and Magistretti, 2009).

1.9.1 Astrocyte classification

Morphologically, astrocytes may be distinguished based on the location in the white versus the gray matter.

Fibrous astrocytes populate the white matter. They typically have regular contours and cylindrical processes, yielding the more classic "starlike" appearance, and have dense glial filaments that stain with the intermediate filament marker GFAP (glial fibrillary acidic protein). Protoplasmic astrocytes populate the gray matter and have more irregular processes and few glial filaments (Vaughn and Pease, 1967; Vaughn and Peters, 1967; Bignami et al., 1972; Freeman, 2010). Protoplasmic astrocytes contact and sheathe synapses by extending thousands of thin processes, with typically only one or two in contact with blood vessels or CNS boundaries (Reichenbach et al., 2010) (Figure 1.5).

In addition, there are two types of specialized astroglia: Bergmann glia in the cerebellum, with cell bodies in the Purkinje cell layer and processes that extend into the granule cell layer, and Muller glia in the retina, whose cells are oriented radially, spanning the photoreceptor layer to the inner retinal surface. Both of these cell types are morphologically reminiscent of the radial glia cells present during CNS

development. However, in the adult CNS, the Bergmann and Muller glia are thought to functionally resemble protoplasmic astrocytes in that they associate with and enwrap synapses and may act to modulate synaptic function (Reichenbach et al., 2010).
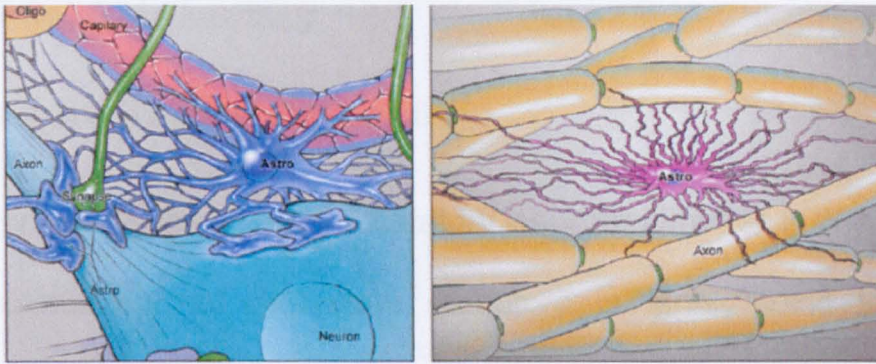
Figure 1.5: Astrocytes are morphologically heterogeneous. (Left) a protoplasmic astrocyte is shown in close connection with a neuron and a capillary, constituting the so-called "neurovascular unit" and highlighting the roles of astrocytes in developmental synaptogenesis and modulating the blood brainbarrier. (Right) a fibrous astrocyte is shown in a white matter tract, where it may interact with oligodendrocytes to promote myelination. Reproduced from (Molofsky et al., 2012)

1.9.2 Astrocyte functions

1) Glutamate uptake and recycling

Glutamate is the primary excitatory neurotransmitter in the brain and overstimulation of glutamate receptors is highly toxic to neurons (Sattler and Tymianski, 2001). While basal extracellular glutamate levels are maintained in the low micromolar range, they increase dramatically during glutamatergic neurotransmission, reaching up to 1 mM in the synaptic cleft. This concentration would cause extensive neuronal injury in the absence of highly efficient mechanisms for its removal at the synapse (Clements et al., 1992). Indeed, activation of the glutamate receptors on neuronal surface results in the opening of an ion channel non-selective to cations. Therefore, persistent activation of postsynaptic receptors drives excess Ca^{2+} into neurons, resulting in "excitotoxicity" that culminate in neuron cell death, once the capacity of the neuron to safely sequester Ca^{2+} is exceeded. Glutamate uptake from the synaptic cleft is primarily accomplished by the astrocyte-specific sodium-dependent high-affinity glutamate transporters GLT-1 and GLAST (corresponding to human EAAT2 and EAAT1, respectively) and to a lesser extent by the neuronal glutamate transporters EAAC1 (human EAAT3) and EAAT4 (Danbolt, 2001).

Indeed, knockout mice for GLT-1, considered the main astrocytic glutamate transporter (it exerts the 90% of glutamate removal), suffer lethal spontaneous seizures and selective hippocampal neuronal degeneration (Tanaka et al., 1997), whereas knockout mice for the neuronal EAAC1 display no apparent neurodegeneration (Peghini et al., 1997). Astrocytes also play a central role in the transfer of glutamate back to neurons following its uptake at the synapse. Failure to do so would result in the rapid depletion of the glutamate pool in presynaptic neurons and subsequent disruption of excitatory neurotransmission. This transfer is achieved by the glutamate-glutamine cycle (Bak et al., 2006; McKenna, 2007). In short, glutamate is converted to glutamine by the astrocyte specific enzyme glutamate-ammonia ligase (GLUL) (Norenberg and Martinez-Hernandez, 1979). Glutamine is then transferred to neurons where it is converted back to glutamate via deamination by phosphate-activated glutaminase, which is enriched in the neuronal compartment (Bak et al., 2006). Astrocytes are also responsible for the replenishment of brain glutamate, as they are the only neural cell type expressing pyruvate carboxylase, a key enzyme allowing them to synthesize glutamate from glucose (Yu et al., 1983) (Figure 1.6, pink box).

2) K+ buffering

Neuronal activity and the resulting propagation of action potentials causes substantial local increases of extracellular potassium ions (K^+) in the restricted extracellular space. Astrocytes are responsible for K^+ buffering through the Na^+/K^+ ATPase pump that enables astrocytes to uptake the excess extracellular K^+. This, can then travel in the astrocyte syncytium through gap junctions from areas of high concentration to areas of lower concentration and finally be extruded into the extracellular space or the circulation (Kofuji and Newman, 2004) (Figure 1.6, orange box).

3) Supply of energy substrates

Neurons have very high energy requirements to maintain the steep ion gradients necessary for the transmission of action potentials (Sokoloff, 1999). Although neurons can import glucose directly from the extracellular space, astrocytes have been proposed to play an instrumental role in coupling neuronal activity and brain glucose uptake through a mechanism referred to as the astrocyte–neuron lactate shuttle (ANLS) (Pellerin et al., 2007). In brief, glutamate uptake by

astrocytes is accompanied by Na$^+$ entry, which is counteracted by the action of the Na$^+$/K$^+$ ATPase. The resulting increase in ADP/ATP ratio triggers anaerobic glycolisis in astrocytes and glucose uptake from the circulation through the glucose transporter GLUT1, expressed specifically by glial and capillary endothelial cells in the brain. Lactate produced by astrocytes as an end result of glycolysis is released into the extracellular space and taken up by neurons. Once into neurons, lactate can be used as an energy substrate via its conversion to pyruvate by the action of lactate dehydrogenase and subsequent oxidation in the mitochondrial TCA cycle. Another key feature of astrocytes is their capacity to store glucose in the form of glycogen. Indeed, in the CNS glycogen is almost exclusively present in astrocytes and virtually constitutes the only energy reserve (Brown and Ransom, 2007) (Figure 1.6, blue boxes).

4) pH buffering

Several neuronal processes are strongly affected by relatively small shifts in pH, including energy metabolism, membrane conductance, neuronal excitability, synaptic transmission, and gap junction communication (Obara et al., 2008). Glial cells (in this case astrocytes

and oligodendrocytes), present a high pH buffering capacity, due to their enriched expression of carbonic anhydrase (CA), which converts CO_2 into H^+ and HCO_3^- effectively allowing them to act as a CO_2 sink. Indeed, during periods of high neuronal activity, the CO_2 produced by elevated oxidative metabolism diffuses into glial cells and is converted to H^+ and HCO_3^- by the action of glial CA. Two HCO_3^- can then be transported into the extracellular space along with one Na^+ via the Na^+/HCO_3^- cotransporter (NBC), thereby increasing the extracellular buffering power. The protons left in the glial compartment can be used to drive the transport of lactate outside of astrocytes through monocarboxylate transporter (MCT) -1 and -4 and its subsequent transport by MCT-2 into neurons, since MCTs exploit proton gradients for the transport of lactate (Deitmer, 2002) (Figure 1.6, yellow box).

5) Defense against oxidative stress

Neuronal activity is associated to a high rate of oxidative energy metabolism, which inevitably generates reactive oxygen species (ROS). However, neurons present a low intrinsic antioxidant capacity, indeed, they are supported, also in this function, by astrocytes which display a much more effective artillery against ROS (Wilson, 1997).

Glutathione (GSH) is the most important antioxidant molecule found in the brain (Dringen and Hirrlinger, 2003). This thiol compound can act as an electron donor, and thus fulfils its antioxidant role either by directly reacting with ROS or by acting as a substrate for glutathione S-transferase or glutathione peroxidase. Both neurons and astrocytes can synthesize the GSH tripeptide (L-glutamyl-Lcysteinylglycine) by the sequential action of glutamate cysteine ligase and glutathione synthetase. However, neurons are highly dependent on astrocytes for their own GSH synthesis. Indeed, astrocytes release GSH in the extracellular space, where it is processed to produce Cys-Gly that is then uptaken from neurons and used for the synthesis of their GSH. The cysteine represents the rate-limiting substrate for GSH synthesis, since neurons, unlike astrocytes, cannot use the cysteine-oxidation product cystine as a precursor (Dringen and Hirrlinger, 2003). The importance of this cooperative process for neuronal defence against oxidative stress is evidenced by the reduced ability of GSH-depleted astrocytes to protect neurons against oxidative injury (Chen et al., 2001). Conversely, increasing the capacity to synthesize GSH in astrocytes specifically by increasing their capacity to uptake cystine significantly enhances the neuroprotective effect of astrocytes against oxidative stress (Shih et al., 2006) (Figure 1.6, green box).

In addition to all these fundamental functions, astrocytes have been found responsible for a process known as "gliotransmission" (Halassa et al., 2007). In brief, astrocytes detect neuronal activity as neurotransmitters that are released into the surroundings and respond to this with a transient increase in their intracellular Ca^{2+} levels, which can travel through the astrocyte syncytium in a wavelike fashion. These Ca^{2+} signals can trigger the release of neuroactive molecules from astrocytes (or gliotransmitters), such as glutamate, D-serine, or adenosine triphosphate (ATP), which in turn may modulate synaptic activity and neuronal excitability (Halassa et al., 2007).
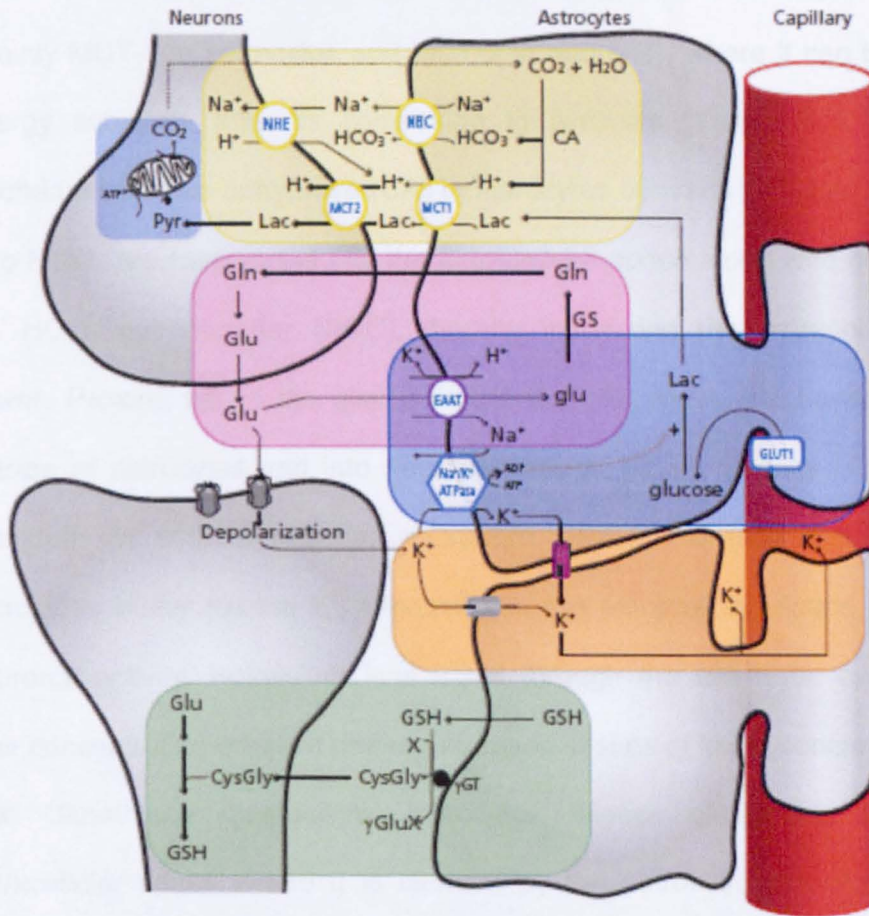
Figure 1.6: **Simplified representation of the main roles of astrocytes in brain homeostasis.** Pink box: glutamate-glutamine cycle. Astrocytic excitatory amino acid transporters (EAATs) are responsible for the uptake of a large fraction of glutamate at the synapse. Glutamate is converted into glutamine by glutamine synthetase enzyme (GS) and shuttled back to neurons for glutamate resynthesis. Blue boxes: Lactate shuttle. Glutamate uptake by astrocytes is accompanied by Na^+ entry, which is counteracted by the action of the Na^+/K^+ ATPase. The resulting increase in ADP/ATP ratio triggers anaerobic glucose utilization in astrocytes and glucose uptake from the circulation through the glucose transporter GLUT1. The

lactate produced is shuttled to neurons through monocarboxylate transporters (mainly MCT-1 in astrocytes and MCT-2 in neurons), where it can be used as an energy substrate after its conversion to pyruvate. Yellow box: pH buffering. Abundant carbonic anhydrase (CA) in astrocytes converts CO_2 into H^+ and HCO_3. Two HCO_3 are transported into the extracellular space along with one Na^+ via the Na^+-HCO_3 cotransporter (NBC), thereby increasing the extracellular buffering power. Protons left in the glial compartment may drive the transport of lactate outside of astrocytes and into neurons through MCTs. Excess H^+ in neurons is extruded via sodium-hydrogen exchange (NHE). Orange box: K^+ buffering. Astrocytes buffer excess K^+ released into the extracellular space as a result of neuronal activity. Potassium ions travel through the astrocytic syncytium down their concentration gradient and are released in sites of lower concentration. Green box: Glutathione metabolism. Astrocytes release glutathione (GSH) in the extracellular space where it is cleaved by the astrocytic ectoenzyme Gamma-glutamyl transpeptidase (GGT). The resulting CysGly serves as a precursor for neuronal GSH synthesis. X represents an acceptor for the gamma-glutamyl moiety in the reaction catalyzed by GGT. Reproduced from (Belanger and Magistretti, 2009).

Aims of the thesis

Astrocytes are the most abundant cell type in the mammalian brain. They play crucial roles in adult CNS homeostasis and, consistently, their impairment is emerging as responsible for neuronal dysfunction in several neurodegenerative diseases (Maragakis and Rothstein, 2006).

The aim of my thesis work was to study the role of astrocytes in the neurological manifestation of Multiple Sulfatase Deficiency, a severe lysosomal storage disorder caused by mutations in the *Sulfatase Modifying Factor 1* (*SUMF1*) gene (Cosma et al., 2003).

To achieve this aim, I had to accomplish the following tasks:

- First, I investigated the cellular consequences of lack of *Sumf1* gene in astrocytes. I used electron microscopy and confocal microscopy to study *in vivo* and *in vitro* the morphology of the lysosomes, the morphology and number of autophagosomes and the accumulation of lysosomal substrates in astrocyte lacking *Sumf1*. I took advantage of the previously generated *Sumf1*$^{-/-}$ mouse line (Settembre et al., 2007).

- To study if lack of *Sumf1* in astrocytes was contributing to the neurodegeneration observed in MSD, I evaluated whether

astrocytes-specific *Sumf1* deletion impaired neuronal survival and function. I addressed this question through two different approaches: i) By using an *ex vivo* co-culture assay I studied the ability of *Sumf1$^{-/-}$* astrocyte to support the survival and function of wild-type cortical neurons; ii) Using the gene targeting in embryonic ES cell and the CRE/Lox techniques, I generated a conditional *Sumf1* knockout mouse line in which *Sumf1* was deleted in astrocyte only (*Sumf1$^{flox/flox}$*; GFAP-Cre) and in both astrocytes and neurons (*Sumf1$^{flox/flox}$*; Nestin-Cre). Then I evaluated cellular morphology and neurodegeneration in different brain regions in both mouse lines at two different ages (6 months and one year).

- Third I studied the neuroinflammation in both *Sumf1$^{flox/flox}$*; Nestin-Cre and *Sumf1$^{flox/flox}$*; GFAP-Cre mouse lines. I performed this analysis by using markers of astrocyte and microglia activation in brain sections.

- Fourth, I investigated whether astrocyte dysfunction is responsible for some of the neurological manifestation of MSD. To address this point I performed a thoroughly behavioural analysis of *Sumf1$^{flox/flox}$*; Nestin-Cre and *Sumf1$^{flox/flox}$*; GFAP-Cre mouse lines.

45

Materials and Methods

2.1 Mice

Sumf1 knockout mice were previously generated (Settembre et al., 2007). The *Sumf1* floxed mouse line was generated as described in the Results section. The mice expressing FLP recombinase were purchased from Jackson Laboratories (strain B6.129S4-*Gt(ROSA)26Sor*$^{tm1(FLP1)Dym}$/JRainJ). GFAP-Cre mice were obtained from National Cancer institute-Mouse Repository (strain name B6.Cg-Tg(GFAP-cre)8Gtm). Nestin-Cre mice were purchased from Jackson Laboratories (strain name B6.Cg-Tg(Nes-cre)1Kln/J). The breeding scheme to obtain *Sumf1*$^{flox/flox}$; Nestin-Cre and *Sumf1*$^{flox/flox}$; GFAP-Cre mice was the following:
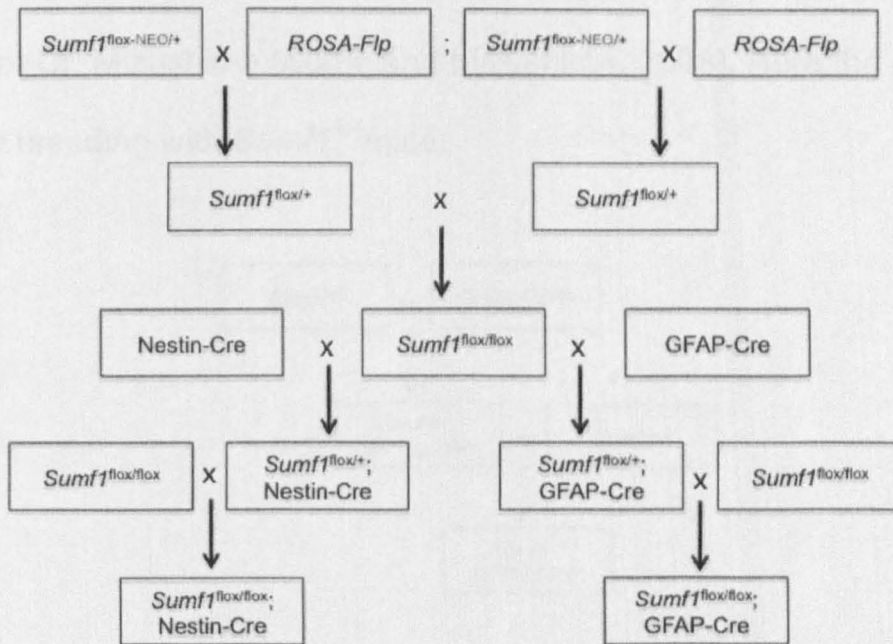
The R26-stop-EYFP mutant mice were purchased from Jackson laboratories (strain name B6.129X1-Gt(ROSA)26Sor$^{tm(EYFP)Cos/J}$) and carried a *loxP* flanked stop sequence followed by the enhanced yellow fluorescent protein (EYFP) inserted into the *ROSA26* locus. Because this transgenic locus was carried in homozygosity, breeding the R26-stop-EYFP mouse with GFAP-Cre mouse was sufficient to obtain the ROSA-EYFP; GFAP-Cre line:

```
  ┌───────────┐     ┌───────────┐
  │ GFAP-CRE  │  X  │ R26-stop- │
  │           │     │ EYFP+/+   │
  └───────────┘     └───────────┘
              │
              ▼
        ┌──────────────────┐
        │   GFAP-CRE;      │
        │ R26-stop-EYFP+/+ │
        └──────────────────┘
```
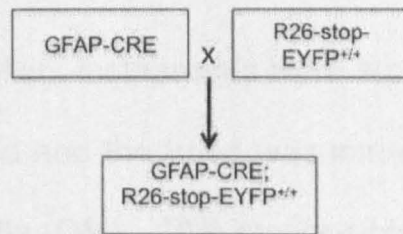
Transgenic line overexpressing GFP tagged LC3 was a generous gift from Dr. Mizushima (Kuma and Mizushima, 2008). Here the scheme of the breeding with *Sumf1$^{+/-}$* mice:

```
  ┌───────────┐     ┌───────────────┐
  │ Sumf1+/-  │  X  │ GFP-LC3tg/tg  │
  └───────────┘     └───────────────┘
              │
              ▼
      ┌──────────────┐     ┌───────────┐
      │  Sumf1+/-;   │  X  │ Sumf1+/-  │
      │ GFP-LC3tg/+  │     │           │
      └──────────────┘     └───────────┘
                   │
                   ▼
             ┌──────────────┐
             │  Sumf1-/-;   │
             │ GFP-LC3tg/+  │
             └──────────────┘
```

48
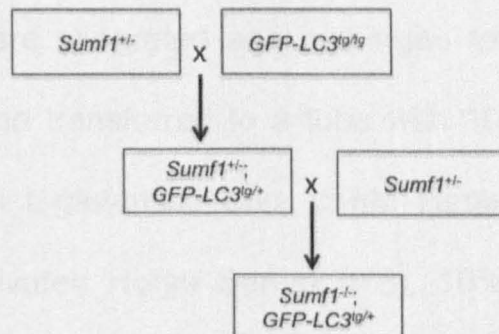
Animal use and analyses were conducted in accordance with the guidelines of the Animal Care and Use Committee of Cardarelli Hospital in Naples and authorized by the Italian Ministry of Health.

2.2 Tissue and cell culture techniques

Astrocyte cultures were prepared from cortex isolated from 1 to 2 postnatal day old $Sumf1^{-/-}$ or $Sumf1^{+/+}$ pups.

For astrocytes isolation, instruments were sterilized in 70% EtOH. The pup was decapitated and the head was immersed in a dish filled with cold dissection media (DM) - 10% glucose-bicarbonate buffer (13.33 g sodium bicarbonate+22.2 g glucose in 500mL water), 1mM sodium pyruvate in 1X HBSS. First, skin and skull were removed from the head and then the brain removed from the ventral side. Subsequently, olfactory bulbs were moved away from the rest of the brain, hemispheres were separated and meninges removed. Cortical lobes were isolated and transferred to a tube with 10mL of plating media - DMEM/F12 with L-glutamine and 15mM Hepes, supplemented with 10% heat inactivated Horse Serum (HS), 10% Fetal Bovine Serum (FBS) and 1 mM sodium pyruvate. Subsequently the media was

aspirated and 1.5 mL of new plating media was added. The tissue was dissociated first using a regular Pasteur pipet, then with a flamed-tip Pasteur pipet with a small opening and subsequently filtered through a Falcon 100 micron cell strainer. One brain (both hemispheres) was plated on 4 four-wells 100 µg/mL poly-D-lysine coated coverslips and cultured in plating media changing the media every 3 days. After 2 weeks in culture, the astrocytes were examinated by immunofluorescence.

For glia-neuron co-culture, cortical neurons from wild-type mouse embryos at E15.5 were isolated as follows: pregnant mouse was anesthetized, then the abdomen was cut and the embryos removed and placed in dissection media. The placenta and the yolk sac were removed, the heads were cut off of the body and the cortices isolated as described before. Neuronal cell culture was prepared similar to astrocytes. Finally, the neuronal preparation was plated on the top of $Sumf1^{-/-}$ or $Sumf1^{+/+}$ astrocytes and cultured for 2 weeks. To inhibit the proliferation of the newly added glial cells eventually contaminating the neuronal preparation, the cytosine arabinoside (10µM) was added 2d after plating neurons. The co-culture was cultured in neuronal media-

MEM supplemented with 10% glucose-bicarbonate buffer, 5% FBS, 5% heat inactivated HS, and 1 mM sodium pyruvate.

2.3 Methods of analysis

2.3.1 Molecular analysis

2.3.1.1 Genotyping

Genotyping was performed on DNA isolated from tail biopsy at the time of weaning. PCR primers used were:

For *Sumf1* $^{-/-}$ mice

primer 1 , 5'- CAAAGTCAGGGTCACAAGGTTCAT-3'

primer 2, 5'- AGAAACCACCTCACCAAAGCAGAG-3'

primer 3, 5'- TTTGTGCCTTTACTGCCCTCTTGG-3'

For GFP-LC3 mice

primer 1 , 5'- ATAACTTGCTGGCCTTTCCACT-3'

primer 2, 5'- CGGGCCATTTACCGTAAGTTAT-3'

primer 3, 5'- GCAGCTCATTGCTGTTCCTCAA-3'

For *Sumf1*^{flox} mice

primer forward, 5'- TGGAGTGGGCAGGTGGAGTCAT- 3'

primer reverse, 5'-CACAGCACGCAGGAACTGTGAG-3'.

For FLP recombinase mice

primer forward, 5'- CACTGATATTGTAAGTAGTTTGC-3'

primer reverse, 5'-CTAGTGCGAAGTAGTGATCAGG-3'

For Nestin-Cre mice

primer forward, 5'- CGCTTCCGCTGGGTCACTGTCG-3'

primer reverse, 5'- TCGTTGCATCGACCGGTAATGCAGGC-3'

For GFAP-Cre mice

primer forward, 5'- GTGTCCAATTTACTGACCGTACAC-3'

primer reverse, 5'- CTAATCGCCATCTTCCAGCAG-3'

For R26-stop-EYFP mice

primer 1, 5'- AAGACCGCGAAGAGTTTGTC- 3'

primer 2, 5'-AAAGTCGCTCTGAGTTGTTAT-3'

primer 3, 5'- GGAGCGGGAGAAATGGATATG-3'

PCR reactions were performed using a standard protocol.

2.3.1.2 Southern Blotting

DNA samples were digested with SpeI or SphI. Ten micrograms of DNA were loaded onto 0.8 % agarose gels. After electrophoresis the gel was treated with 0.5M NaOH, 1.5M NaCl denaturing solution for 30 min, then 30 min in 0.5M Tris-HCl, 1.5M NaCl neutralization solution. The gel was then equilibrated for 20 min in 20x SSC solution (3M NaCl, 300mM sodium citrate-$2H_2O$). DNA was transferred overnight onto Ni^+ (Roche) membranes using capillary blotting with 20 X SSC buffer. The membrane was then crosslinked with 120mJ UV and hybridized with the respective 32P-dCTP labelled probe in Church buffer (0.25mM sodium phosphate buffer, 1mM EDTA, 1% BSA, 7% SDS) over night. Radioactive labelling of the probe was carried out using High Prime labelling kit (Roche) according to manufacturer instruction. After washing with 2 x SSC buffer 30 min, 1 x SSC buffer 30 min and 0.5 x SSC buffer 10 min the hybridization signal was detected with BAS 2000 BioImaging Analyser (FujiFilm).

2.3.1.3 Gene Expression Analysis

Freshly dissected hemi-brains cut along the mouse brain's midline (n= 3 mice/genotype, 6 months of age) were placed in 2 ml Trizol (Invitrogen) on ice and immediately homogenized with Polytron homogenizer. Total RNA was cleaned and DNA removed with on-column DNase digestion using the Qiagen RNeasy Mini kit (Qiagen Inc). Quantitec (Qiagen) was used to synthesize first-strand cDNA from 1μg purified total RNA. Quantitative PCR was performed using Applied Biosystems 7300 Real Time PCR System (Applied Biosystems). Quantitative PCR reactions were conducted in triplicate and the results were averaged for each sample and normalized to *cyclophilinA* levels.

Indeed, cyclophilins are cytosolic, highly abundant proteins and *cyclophilinA* gene was used as housekeeping gene since its level was not changing among the different genotypes.

RT-PCR primers used were:

*CyclophilinA*_forward, 5'- GGCAAATGCTGGACCAAACACAA- 3'

*CyclophilinA*_reverse, 5'- GTAAAATGCCCGCAAGTCAAAAG- 3'

*Gapdh*_forward, 5'- GTCTCCTCTGACTTCAACAGCG- 3'

*Gapdh*_reverse, 5'- ACCACCCTGTTGCTGTAGCCAA- 3'

*Mip1α (CCL3)*_forward, 5'- ACTGCCTGCTGCTTCTCCTACA- 3'

*Mip1α (CCL3)*_reverse, 5'- ATGACACCTGGCTGGGAGCAAA- 3'

*Mip1β (CCL4)*_forward, 5'- ACCCTCCCACTTCCTGCTGTTT- 3'

*Mip1β (CCL4)*_reverse, 5'- CTGTCTGCCTCTTTTGGTCAGG- 3'

*TNFα*_forward, 5'- GGTGCCTATGTCTCAGCCTCTT- 3'

*TNFα*_reverse, 5'- GCCATAGAACTGATGAGAGGGAG- 3'

2.3.2 Biochemical analysis

2.3.2.1 Sulfatase enzymatic assays

Specimens were resuspended in water and then disrupted by 3 cycles of freeze-thaw. Then, samples were centrifuged at 13000rpm with a benchtop centrifuge for 15 min at 4°C and the supernatant, containing the protein fraction, transferred to a new tube. Protein concentration was measured using Bradford protein assay according manifacturers' instructions (Bio-Rad). For all enzyme activity assays, 30µg of proteins were incubated at 37°C for 3 hr under the specific assay conditions.

For ARSA assay, homogenates were incubated with 0.02M p-nitrocatechol sulfate in 0.5M acetate buffer (pH 5) containing 0.85M NaCl and 0.25mM sodium pyrophosphate in an incubation volume of 0.3ml. The reaction was stopped with 0.7ml 0.64N NaOH and absorbance was read at 515nm on a Perkin Elmer spectrophotometer. For ARSB and ARSC enzymatic activity the 4-methylumbelliferyl (4-MU) sulfate was used as substrate. ARSB activity was determined by incubating cell homogenates with 6.25mM 4-MU sulfate in 0.375mM $AgNO_3$ 0.1M NaOAc buffer (pH 5) in 80µl of incubation mixture. ARSC was measured by incubating cell homogenates with 0.2mM 4-MU sulfate in 0.25% Triton X100, 0.05 M phosphate buffer (pH 8) in 0.2ml incubation volume. For ARSB and ARSC the reactions were stopped with 2ml glycine-carbonate buffer pH (10.7) and fluorescence was read at 365nm (excitation) and 450nm (emission) on a Turner fluorometer. Statistical analyses of the measurements were analyzed using Student's t-test. Data are shown as mean ± standard error of mean.

2.3.3 Histological analysis

2.3.3.1 Electron microscopy

Mice at 3 and 6 months of age were injected intraperitoneally with 20 mg/mL Avertin and then subjected to intracardial perfusion using PBS for 2 min, and then 2.5% gluteraldehyde, 2.0 % paraformaldehyde in 0.1M phosphate buffer for 15 min- flow rate: 10mL/min. After perfusion, brain was removed, cortex isolated and cut into 1mm cubes and immediately immerse in fixative solution for 2-3 hours on shaker. From here, preparation of samples for Electron microscopy was performed in collaboration with Electron microscopy Core at Baylor College of Medicine.

Briefly: specimens were washed 3x 5 min each with 0.1 M phosphate buffer, pH7.2-7.4, post fixed for 1-2 hr in 1% OsO4 in 0.1 M phosphate buffer, washed again 3 x 5 min each with 0.1 M phosphate buffer, then gradually dehydrated with increasing concentration of ETOH and subsequently gradually infiltrated with Spurr's resin. Finally, ultra-thin sections of approximately 70nm were obtained using an RMC MT6000-XL ultramicrotome and a Diatome Ultra45 diamond knife, and collected on 150 hex-mesh copper grids. The ultra-thin sections were then stained with Reynold's lead citrate for 4 minutes. I examined the

air-dried samples on a Hitachi H7500 transmission electron microscope and I captured images using Gatan US1000 digital camera and Digital Micrograph v1.82.366 software.

I distinguished the different cell populations of the brain according morphological criteria (Patricia C. Cross, 1993). Briefly, glial cells were distinguished from neurons by their smaller, more irregular shape and for the prominent differences in the nucleus, devoid of nucleolus and with a condensed envelope. Astrocytes can be distinguished from other glial populations since they contain a characteristic intermediated-sized filament composed of glial fibrillary acidic protein (GFAP) and compared to oligodendrocytes are usually bigger and with a paler, euchromatic nucleus. Microglial cells are very similar to macrophages in morphology and they are the smallest cells within the CNS with an irregular shape and a darker cytoplasm.

2.3.3.2 Immunofluorescence and Immunohistochemistry

For immunofluorescent staining of mouse brain sections, mice at 3 and 6 months of age were injected intraperitoneally with 20 mg/mL Avertin and then subjected to intracardial perfusion using PBS for 2 min and

then 4% paraformaldehyde (PFA) in PBS for 15 min- flow rate: 10mL/min. Brains were dissected and post-fixed with buffered 4% PFA overnight at 4°C, then washed with PBS and cryoprotected in successive sucrose solutions diluted with PBS: 5% for 30 minutes, 10% for several hours, and 20% overnight at 4°C; finally embedded in OCT. Cryostat sections were cut at 30μm or 50μm (floating sections). For immunofluorescence floating sections were blocked and permeabilized in 3% BSA, 5% goat serum in PBS + 0.3% Triton X-100 for 3h, then incubated with the primary antibody overnight. Sections were washed 3 times with 3%BSA in PBS + 0.3% Triton X-100, and then incubated for 3 h with secondary antibodies conjugated with Alexafluor 488, or Alexafluor 555, or Alexafluor 633. For immunofluorescence of astrocyte culture or astrocyte-neuron coculture, cells were washed twice in PBS then fixed with cold buffered 4% PFA for 15' at room temperature (RT), then permeabilized with PBS + 0.2% Triton for 30' at RT and blocked in 3% BSA, 5% HS in PBS + 0.1% Triton. The primary antibody was added overnight, washed with PBS and incubated with secondary antibodies. Images were captured using a Leica SP5 Confocal microscope and quantitave analysis performed using Image J software.

For Immunohistochemistry, after being post-fixed with buffered 4% PFA overnight at 4°C, brains from 6 and 12 months old mice were dehydrated in a graded series of ethanol: 70% ethanol for 1 hour; 95% ethanol for 2 hours; 100% ethanol for 2 hours; then cleared with Xylene for 30 minutes, 1 hour and then a further 1 hour (changing the solution between each time period). Finally, the specimens were infiltrated with paraffin for 1 hour, and then over night. Paraffin-embedded blocks were cut on a microtome in 5 µm sections. Sections were then deparaffinized in two changes of xylene followed by two changes of absolute ethanol, two changes of 95% ethanol, one of 70% and then rehydrated in tap water. Endogenous peroxidase activity was quenched by incubating the sections for 30 minutes in 0.3% H_2O_2 in water. Sections were then washed in PBS buffer for 5 min and subsequently incubated for 20 min with blocking solution (1,5 % horse serum in PBS). Incubation with primary antibodies (anti-Neun or anti-calbindin) was done overnight at 4 °C in blocking solution, after which they were incubated with a biotinylated horse anti-mouse secondary antibody in PBS-1,5% horse serum. Secondary antibodies were visualized using avidin–biotin–horseradish peroxidase complex (Vectastain ABC kit, 1:100 inPBS, Vector Labs, Burlingame, CA) for 30 min followed by a PBS wash (3 x 5min), 0.05% 3,3-diaminobenzidine

tetrahydrochloride (DAB) and 0.02% H2O2 for 20 min, and a final PBS wash (3 x 5min). Bright field images were taken using a Zeiss Axioplan 2 imaging microscope. Images were acquired with a high-resolution color digital camera (Axio cam) using the Zeiss AxioVision software.

2.3.3.3 Neuronal quantification

For the cortical neurons and Purkinje cell quantification, three sagittal sections/mouse (5µm thickness) starting from the median sagittal plane were used. Bright field images were taken using a Zeiss Axioplan 2 imaging microscope. Images were acquired with a high-resolution color digital camera (Axio cam) using the Zeiss AxioVision software. The counts were performed using a 200 X 200 µm grid throughout the section area. Five mice for genotype were used. The cortical layers were defined as follows: layers II-III, 150 µm from the surface to a depth of 350µm; layer IV, 350-550µm; layer V, 550-750µm (Hampton et al., 2010). Purkinje cells were quantified within a defined region of the cerebellum (VIII lobe). NeuN- and Calbindin- positive cells were quantified with the Imagej software analysis using the Cell Counter plugin with a fixed threshold. All studies were carried out with the observer blinded to genotype.

2.3.3.4 Nissl staining

Nissl staining typically marks the ER due to ribosomal RNA, so it stains both neurons and glia. Briefly, 5µm paraffin embedded sections from 6 months old mouse brain were stained in 0.1% cresyl violet solution for 5 minutes, then rinsed quickly in distilled water and differentiated in 95% ethyl alcohol for 15 minutes; finally they were cleared in xylene and mounted with permanent mounting media.

2.3.3.5 Markers and Antibodies

GFAP: standing for Glial fibrillary acidic protein, is the characteristic astrocyte intermediate filament, whose expression is increased during astrocyte activation (Brenner et al., 1994). Therefore GFAP marker is used to mark astrocyte cells. Antibodies used for GFAP antigen were: Polyclonal rabbit anti-GFAP (Dako, cat. Z0334, dilution 1:500) and Monoclonal anti-GFAP antibody produced in mouse (Sigma, cat. G3893, dilution 1:500).

Ubiquitin: original name ubiquitous immunopoietic polypeptide, is a small polypeptide which binds to proteins for degradation, via proteosomal or autophagic pathway. Ubiquitin-positive aggregates

represent storage of poly-ubiquitinated proteins that accumulates in cells with impairment of autophagy (Hara et al., 2006; Komatsu et al., 2006). The antibody used for ubiquitin antigen was: Polyclonal rabbit anti-Ubiquitin (Dako, cat. Z0458, dilution 1:250)

NeuN: standing for "neuronal nuclei" is a neuron-specific nuclear protein, originally identified by immunoreactivity with a neuronal specific monoclonal antibody, anti-NeuN. It was recently identified as the Fox-3 gene product, whose expression is indeed specific for neuronal cells where it functions as a splicing regulator (Kim et al., 2009). The antibody used for NeuN antigen was Mouse Anti-NeuN, clone A60 (Millipore, cat. MAB377, dilution 1:500).

GFP-LC3: stands for GFP-tagged LC3 protein (Kuma and Mizushima, 2008). LC3 is an abbreviation for MAP1LC3A, the mammalian homologue of yeast ATG8, an important marker and effector of autophagy. LC3 is present in two forms in the cell, the cytosolic soluble LC3-I form and the autophagosome-complexed form LC3-II. During autophagy, LC3-I is lipidated becoming LC3-II and localizes in the inner membrane of the rising autophagosome (phagophore) where it recruits autophagic substrates and is itself degradeted via autophagy. Therefore, accumulation of LC3-positive dots into the cells represents

accumulation of autophagosomes (Kabeya et al., 2000). Beacause LC3 was fused with GFP (green fluorescent protein) the antibody used for detect LC3 was Chicken polyclonal to GFP (Abcam, cat. ab92456, dilution1:500).

SQSTM1/ P62: stands for Sequestosome-1 (P62 because of its molecular weight, 62 kDa). Similarly to LC3, P62 is both an effector and a substrate of autophagy: through its two binding domains, one for LC3 and the other for ubiquitin, it targets polyubiquitinated proteins to the autophagosomes for autophagy degradation. Therefore its intracellular accumulation often indicates impairment in autophagy process (Mizushima et al., 2010). The antibody used for SQSTM1/ P62 was Monoclonal Mouse anti-SQSTM1 (BD Bioscience, cat. 610833, dilution 1:1000)

Calbindin: full name, Calbindin-D28k, is a calcium-binding protein belonging to the troponin C superfamily. In the brain, it marks Purkinje cells (Whitney et al., 2008). The antibody used for calbindin was Monoclonal Anti-Calbindin-D-28K antibody produced in mouse (Sigma, CP848, dilution 1:200).

MAP2: Microtubule-associated protein 2, is a neuron-specific protein that stabilizes microtubules in the dendrites of postmitotic neurons (Izant and McIntosh, 1980).

The antibody used for MAP2 was Anti-MAP2A Antibody, 2B, produced in mouse (Millipore, cat. MAB378, dilution 1:200).

F4/80: *F4/80* gene is the mouse homologue of the human gene *EMR1* (EGF-like module-containing mucin-like hormone receptor-like 1), which encodes a transmembrane protein present on the cell-surface of macrophages. Therefore, it is a marker of microglia activation (Perry et al., 1985). The antibody used for F4/80 was rat anti mouse F4/80 (AbD Serotec, cat. MCA497R, dilution 1:100).

The secondary antibodies used were: Alexa Fluor Secondary Antibodies, purchased from Invitrogen and used at a dilution of 1:500.

2.3.4 Behavioural analysis

All behavioural studies were carried out with the observer blinded to genotype. The mice were 7 months old and the number (*n*) used per genotype is noted in the corresponding figure legend. For all studies, the mice were allowed to habituate to the testing room for 30 minutes

prior to testing.

Accelerating rotarod: Mice were placed on an accelerating rotarod apparatus (Ugo Basile) for 8 trials (four trials/day on two consecutive days) with a 60-minute rest interval between trials. Each trial lasted for a maximum of 5 min, during which the rod accelerated linearly from 4 to 40 rpm. The amount of time for each mouse to fall from the rod was recorded for each trial. Data are shown as mean ± standard error of mean and analyzed with two-way ANOVA (genotype x trial) with repeated measures and Tukey's post hoc analysis.

Parallel Rod Footslip Test with ANY-maze

The parallel rod footslip test was used to assess motor incoordination in mice. The apparatus is adapted from Kamenset al., 2005 and was used in conjunction with a special version of ANY-maze to simultaneously assess ataxia and locomotor activity. Footslips were detected when a paw touched a metal plate below the parallel rod floor completing a circuit that was registered by the system. Locomotor activity was measured by the ANY-maze tracking software using an overhead camera. Test time was set for 10 min. Data are shown as mean ± standard error of mean and analyzed by one-way ANOVA with

Tukey's post hoc analysis.

Open Field Assay

The open field apparatus consisted of a clear, open Plexiglas box (40 × 40 × 30 cm) with photo beams to record horizontal and vertical movements of the mouse. Overhead lighting was set at 200-lux illumination and a white noise generator (Lafayette Instruments, Lafayette, IN) maintained a 60dB background noise. Mice were placed in the center of the box. Activity was quantified over a 30 minute period by a computer-operated Digiscan optical animal activity system (Accuscan Electronics, Columbus, OH). Data are shown as mean ± standard error of mean and analyzed by one-way ANOVA with Tukey's post hoc analysis.

Light Dark Box

The box consisted of a clear Plexiglas chamber (36 × 20 × 26 cm) with an open top separated from a covered black chamber (15.5 × 20 × 26 cm) by a black partition with a small opening. Overhead lighting was maintained at 700lux illumination and white noise was maintained at 60dB. Mice were placed into the illuminated side and allowed to explore freely for 10min. A hand-held computer (Psion Workabout mx,

Psion Teklogix) and the Observer program (Noldus Information Technologies) were used to score the mice for the number and latency of entries and the time spent in each compartment. Mice with all four feet placed into either the light or dark compartment were scored as an entry. Data are shown as mean ± standard error of mean and analyzed by one-way ANOVA with Tukey's post hoc analysis.

Results

3.1 Lysosomal storage and autophagy dysfunction in astrocytes of $Sumf1^{-/-}$ mice

I first investigated the cellular consequences in astrocytes of global $Sumf1^{-/-}$ mice. Transmission electron microscopy revealed that 3 months old $Sumf1^{-/-}$ brain cortical astrocytes presented massive cytoplasmic vacuolization (Figure 3.1a) representing lysosomes containing disperse and flocullar material (arrow), and autolysosomes filled with partially digested cytoplasm (arrowhead), suggesting a defect in degradation of autophagic cargo secondary to the lysosomal storage. Subsequently, co-immunolabelling of astrocytes with GFAP and ubiquitin antibodies showed the accumulation of ubiquitin positive aggregates in the cytoplasm of astrocytes of $Sumf1^{-/-}$ mice compared to control (Figure 3.1b). A similar phenotype was observed in neurons and microglia of $Sumf1^{-/-}$ mice (Figure 3.2a-c).
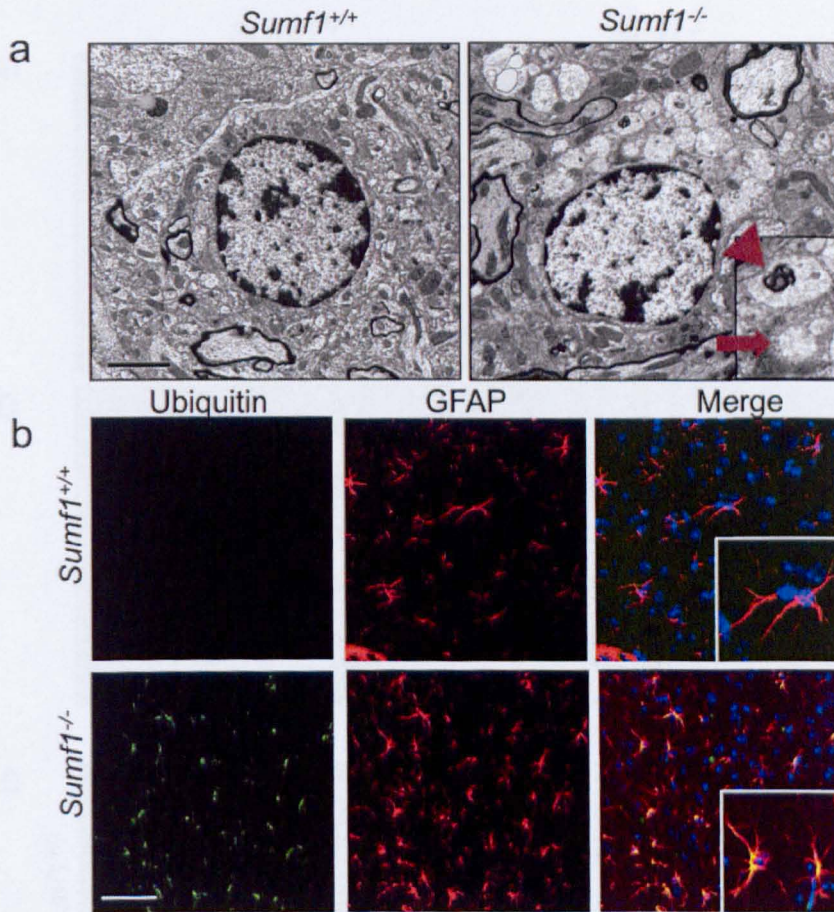
Figure 3.1: Lysosomal storage and autophagy dysfunction in *Sumf1*^{-/-} astrocytes (a) Lysosomal storage in *Sumf1*^{-/-} astrocytes. Electron micrograph showing large vacuoles in the cytoplasm of astrocytes of 3 months old *Sumf1*^{-/-} mice (right). Astrocytes from control mice (left) did not show signs of vacuolization. Enlargement shows lysosomes containing disperse and floccular material (arrow), and autolysosomes filled with partially digested cytoplasm (arrowhead). (b) Astrocytes from *Sumf1*^{-/-} mice accumulate ubiquitin positive cytoplasmic aggregates. Frozen cortical tissue isolated from 3 months old *Sumf1*^{-/-} and control mice immunostained with ubiquitin (green) and GFAP (red) antibodies. [Scale bars: 2 µm (a); 10 µm (b)]
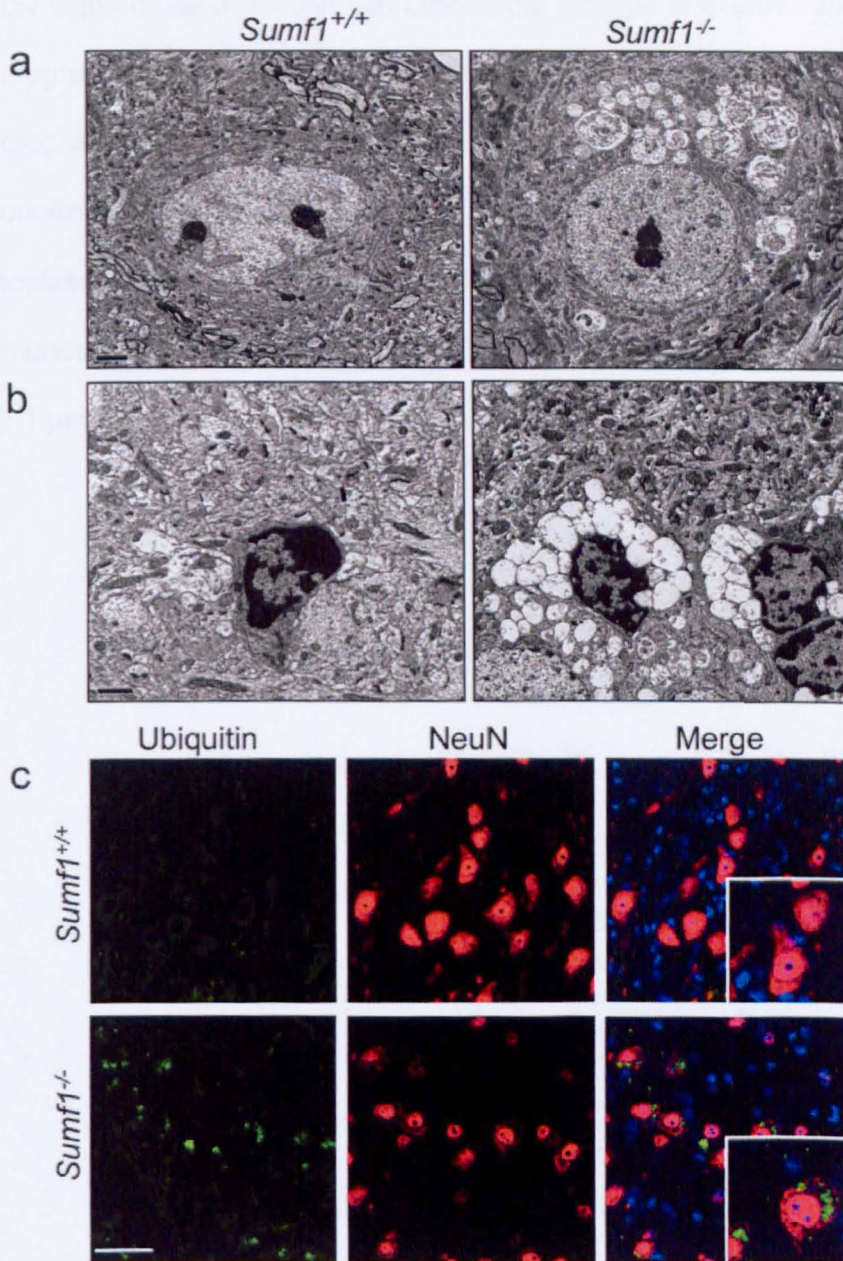
Figure 3.2: Lysosomal dysfunction in *Sumf1⁻ᐟ⁻* neurons and microglia (a) Lysosomal storage in *Sumf1⁻ᐟ⁻* neurons. Electron micrograph showing large vacuoles, mainly autolysosomes filled with undigested material in the cytoplasm of neurons from 3 months old *Sumf1⁻ᐟ⁻* mouse (right). Control neurons (left) do not

show signs of vacuolization. (b) Lysosomal storage in *Sumf1*$^{-/-}$ microglia. Electron micrograph from cortex of 3 months old *Sumf1*$^{-/-}$ mouse shows highly vacuolized microglia (right). Microglia from a control mouse (left) does not show signs of vacuolization. (c) Accumulation of ubiquitin positive aggregates inside the cytoplasm of neurons. Brain tissues from 3 months old *Sumf1*$^{-/-}$ and control mice immunostained with ubiquitin (green) and NeuN (red) antibodies. [Scale bars: 2 µm (a); 1 µm (b); 10 µm (c).]

To evaluate whether this substrate accumulation is the consequence of impaired autophagy (Hara et al., 2006; Komatsu et al., 2006), I isolated cortical astrocytes from control and *Sumf1*^-/- mice harbouring a transgene expressing a GFP-tagged LC3 protein (Kuma and Mizushima, 2008), a well-established marker for autophagosomes (Kabeya et al., 2000). The cytoplasm of astrocytes from *Sumf1*^-/- mice had abundant accumulation of large GFP-positive autophagosome vesicles (Figure 3.3a). Moreover I observed a cytoplasmic increase of P62/*SQSTM1*, a known substrate of autophagy whose accumulation induces cellular toxicity (Figure 3.3b) (Zatloukal et al., 2002; Bjorkoy et al., 2005). These data are consistent with a model in which autophagy is impaired rather than induced in LSD cells, suggesting that astrocytes from *Sumf1*^-/- mice accumulates toxic substrates as a result of a lysosomal degradation defect.
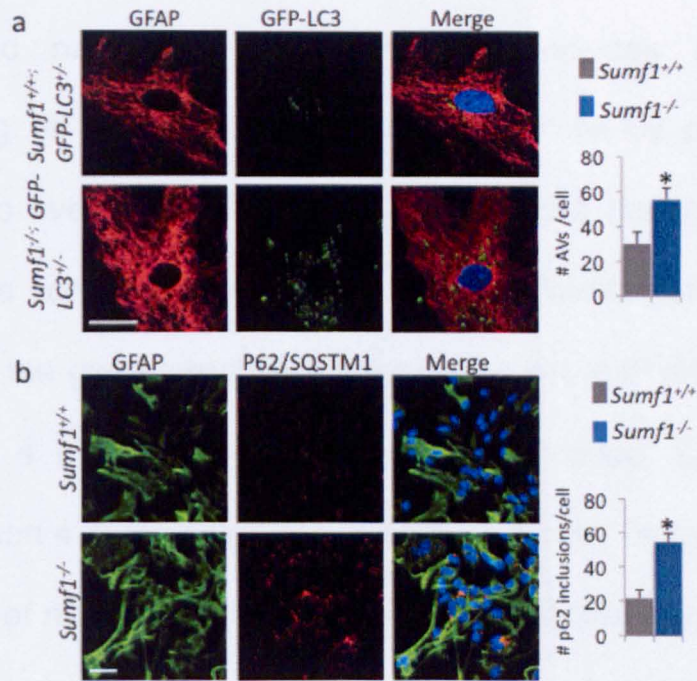
Figure 3.3: Autophagy impairment in *Sumf1⁻ᐟ⁻* astrocyte. (a) Primary astrocytes isolated from *Sumf1⁻ᐟ⁻*; GFP-LC3 and *Sumf1⁺ᐟ⁺*; GFP-LC3 pups were stained with GFP (green) and GFAP (red) antibodies. Histogram shows the number of GFP positive vesicles (representing autophagosomes) per cell. (b) Primary astrocytes isolated from *Sumf1⁻ᐟ⁻* and control mice were stained with GFAP (green) and P62/*SQSTM1* (red) antibodies. Histogram shows the quantification of P62 positive puncta per cell. (Astrocytes were isolated from at least three mice/genotype; at least 15 cells/mice were counted. Error bars represent standard deviation; *, Student's t test $P < 0.05$). [Scale bars: 5 µm]

3.2 Generation of *Sumf1*^{flox} mice

The systemic nature of MSD disease precludes a complete understanding of the neuronal dysfunction *per se* by using *Sumf1* global KO. To overcome this issue, I generated a transgenic mouse line carrying a conditional null mutation in the *Sumf1* gene (*Sumf1*^{flox} mice). I used the gene targeting strategy to insert *loxP* sites on either side of exon 4 (Figure 3.4a, green arrows). Indeed, Cre-mediated excision of exon 4 is predicted to cause a frameshift mutation and the incorporation of multiple stop codons. The conditional targeting vector for *Sumf1* gene was constructed using a BAC containing the C57BL/6J *Sumf1* genomic clone. A fragment spanning from intron 3 to intron 6 of *Sumf1* was subcloned into PL253 (a pBluescript derived plasmid) via recombineering (Copeland et al., 2001) using EL350 bacteria cells (a derived strain of DH10B cells, carrying the temperature inducible Red genes). Subsequently the *loxP* site upstream the exon 4 was cloned into the plasmid by introducing a floxed neomycin resistance (Neo) cassette (amplified from PL452 plasmid) via homologous recombination. Then the resistance cassette was removed via Cre recombinase, leaving a single *loxP* site at the targeted locus. The insertion of the second *loxP* site was accomplished using a neomycin

cassette flanked with two *FRT* sites (Figure 3.4a, black arrows) and one *loxP* site following the second *FRT* (amplified from PL451 plasmid); the *Sumf1* targeting vector was linearized with NotI and electroporated into Bruce4 mouse embryonic stem cells, and the G418-resistant clones were screened by Southern Blot using the strategy shown in Figure 3.4a. Euploid clones that had undergone homologous recombination were injected into albino C57BL6/J blastocysts. Germline transmission of the floxed allele in offspring was confirmed by Southern blot (Figure 3.4b). To remove the Neo cassette, the resulting mice were crossed with mice expressing FLP recombinase.
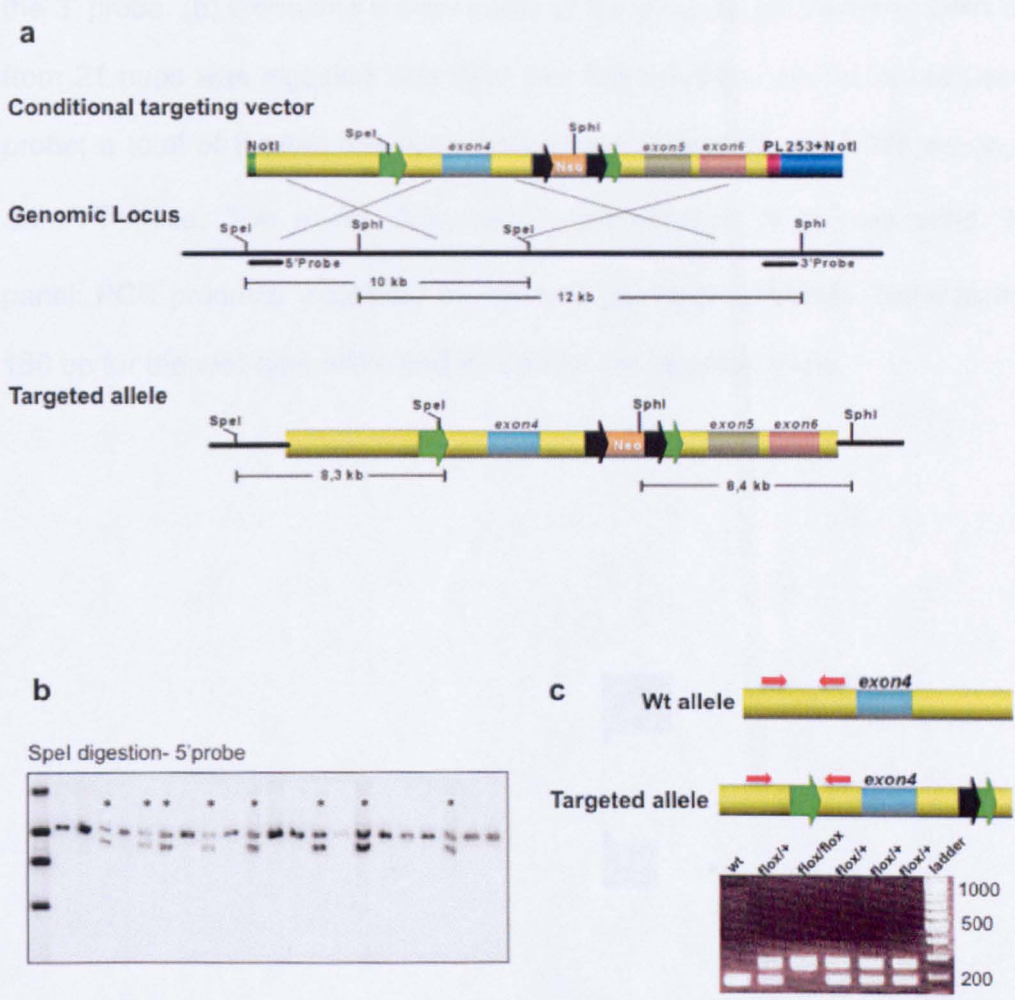
Figure 3.4: Generation of the conditional knockout (CKO) *Sumf1* mouse line

(a) Schematic representation of the homologous recombination event between the *Sumf1* targeting vector and the *Sumf1* genomic locus. Correctly targeted ES cells (CKO allele) have a 8.3kb SpeI band, in addition to a 10kb wild-type band, following hybridization with the 5' probe. These CKO clones also have a 8.4kb SphI-targeted band, as well as a 12kb wild-type band following hybridization with

the 3' probe. (b) Germ-line transmission of the CKO allele. Genomic DNA derived from 21 pups was digested with SpeI and the Southern blot analyzed using a 5' probe; a total of 8 germ-line mice were found (asterisks). (c) PCR genotyping of *Sumf1*[flox] mice. Top panel: Schematic representation of primers used. Bottom panel: PCR products visualized by agarose gel electrophoresis. Band sizes were 180 bp for the wild-type allele and 250 bp for the targeted allele.

3.3 Deletion of *Sumf1* gene in neuronal precursor derived cells or in astrocytes

To analyze neuronal dysfunction in MSD and dissect the contribute of astrocyte impairment, I generated two mouse lines: one in which *Sumf1* was deleted in neuronal precursor derived cells (NPCs -both neurons and glia) which was obtained by crossing a transgenic mouse that expresses the Cre recombinase under the control of the nestin promoter with the *Sumf1*^flox/flox mouse (*Sumf1*^flox/flox; Nestin-Cre) and the other in which *Sumf1* was deleted only in astrocytes, obtained using a transgenic mouse expressing the Cre recombinase under the control of the GFAP promoter (*Sumf1*^flox/flox; GFAP-Cre). I selected a GFAP-Cre line that was recently shown to be astrocyte specific (Weidemann et al., 2009). I first verified that this transgenic line is indeed specific for astrocytes by crossing it with a *ROSA26-EYFP* reporter mouse line and I observed that the YFP colocalized with the astrocyte marker GFAP, but not with the neuronal marker NeuN (Figure 3.5a-c).
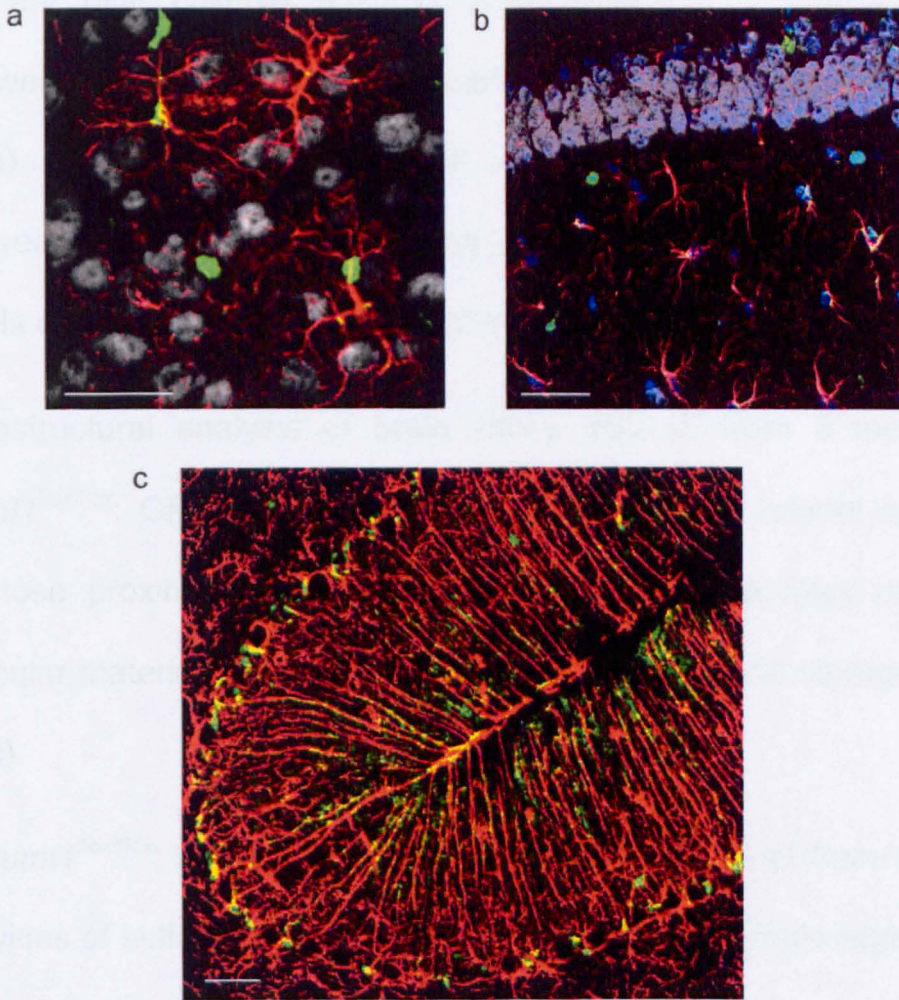
Figure 3.5: Specificity of GFAP-Cre transgenic line. (a,b) YFP protein colocalizes with the GFAP marker for astrocytes and not with the neuronal marker NeuN in GFAP-Cre[+]; Rosa-YFP [+/-] mouse. Immunostaining using GFP antibody (green), GFAP-antibody (red) and NeuN-antibody (grey) from cortex (a) and hippocampus (b). (c) Colocalization of YFP protein (green) with GFAP marker (red) in the Bergmann glia of cerebellum in GFAP-Cre[+]; Rosa-YFP [+/-] mouse. [Scale bars: 20 µm]

Primary glial cultures isolated from *Sumf1*^{flox/flox}; GFAP-Cre mice showed an almost complete lack of *Sumf1* mRNA expression (Figure 3.6a) and virtually no residual sulfatase activities (Figure 3.6b), whereas primary cortical neurons from the same mice had normal levels of *Sumf1* mRNA and normal sulfatase activities (Figure 3.6a,b).

Ultrastructural analysis of brain slices isolated from 6 months old *Sumf1*^{flox/flox}; GFAP-Cre mice showed neurons with normal cytoplasm in close proximity to astrocytes with enlarged vacuoles containing floccular material, which are typical signs of lysosomal storage (Figure 3.6c).

In *Sumf1*^{flox/flox}; Nestin-Cre both the expression levels of *Sumf1* and the activities of sulfatases were almost undetectable in whole brain lysates (Figure 3.6d,e). Accordingly, at 6 months of age, the cytoplasm of neurons and astrocytes had extensive vacuolization, representing enlarged lysosomes and autolysosomes containing undigested material (Figure 3.6f).

Sumf1^{flox/flox}; Nestin-Cre and *Sumf1*^{flox/flox}; GFAP-Cre mice were born at Mendelian ratios, and indistinguishable in appearance from control littermates. However, I observed significant weight loss in *Sumf1*^{flox/flox}; Nestin-Cre starting from 3 months of age and even more evident at 6

months of age (Figure 3.7a), whereas no difference in body weight was observed in $Sumf1^{flox/flox}$; GFAP-Cre mice compared to their control littermates. Both genotypes showed signs of neurodegeneration as early as 6 months of age, including abnormal limb-clasping reflexes (Figure 3.7b), tremor, and epileptic episodes. Behavioral abnormalities were also assessed at 7 months of age (as described in section 3.7). The onset of symptoms for the two mouse lines is reported in Table 3.1.

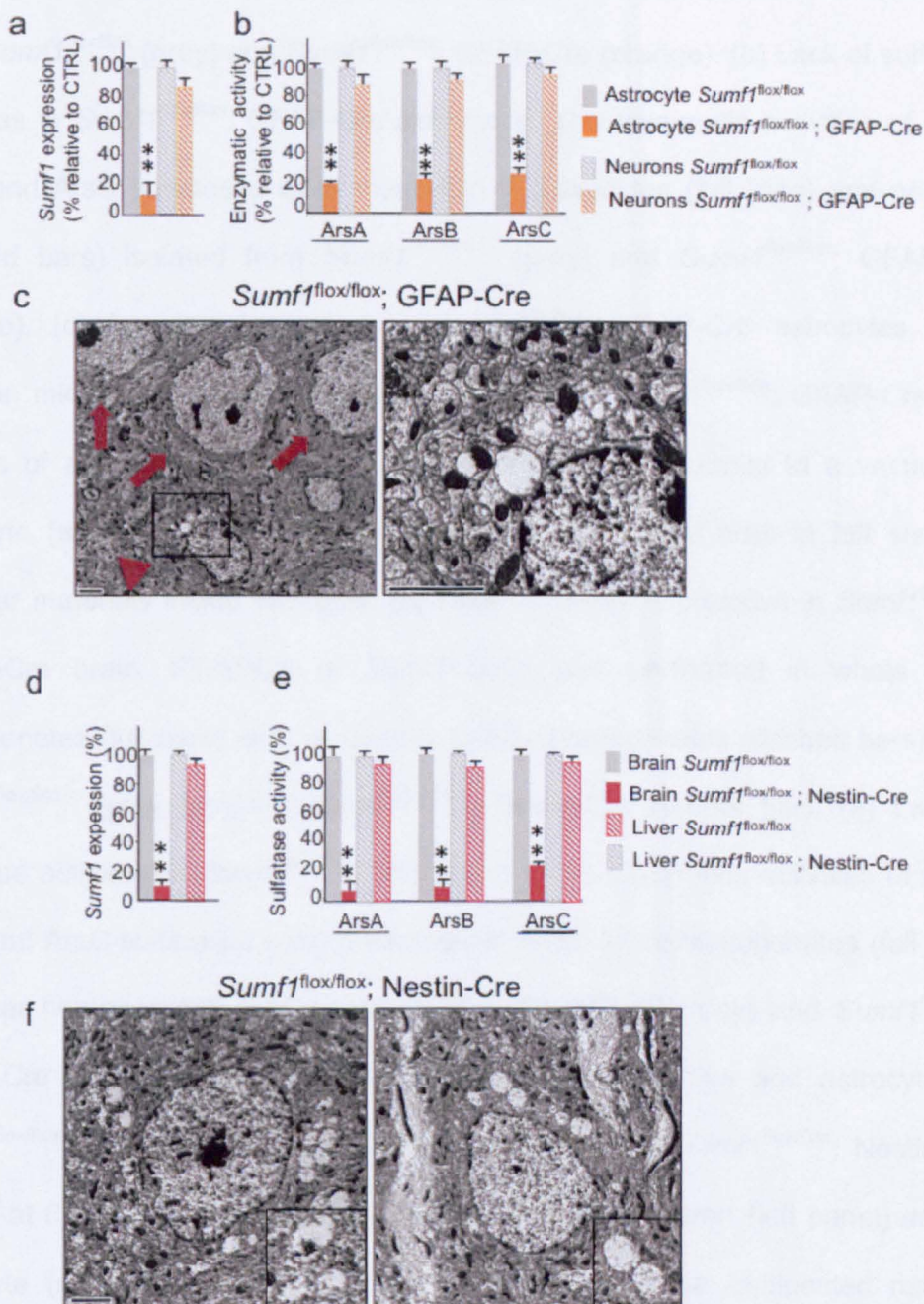**Figure 3.6: Lysosomal storage in *Sumf1*^flox/flox^; GFAP-CRE and *Sumf1*^flox/flox^; Nestin-Cre mouse lines** (a) Lack of *Sumf1* expression in *Sumf1*^flox/flox^; GFAP-Cre astrocytes. Reverse transcription followed by quantitative PCR (RT-qPCR) of

Sumf1 gene expression in astrocyte (full bars) and neurons (dashed bars) isolated from *Sumf1*$^{flox/flox}$ (grey) and *Sumf1*$^{flox/flox}$; GFAP-Cre (orange). (b) Lack of sulfatase activities in *Sumf1*$^{flox/flox}$; GFAP-Cre astrocytes. The enzymatic activities of ArsA, ArsB and ArsC sulfatases were measured in astrocytes (full bars) and neurons (dashed bars) isolated from *Sumf1*$^{flox/flox}$ (grey) and *Sumf1*$^{flox/flox}$; GFAP-Cre (orange). (c) Lysosomal storage in *Sumf1*$^{flox/flox}$; GFAP-Cre astrocytes. (left) Electron micrograph of cortical tissue isolated from *Sumf1*$^{flox/flox}$; GFAP-Cre at 6 months of age showing healthy neurons (arrows) in proximity to a vacuolized astrocyte (arrowhead). (right) Enlargement of the boxed area in left showing floccular materials inside vacuoles. (d) Lack of *Sumf1* expression in *Sumf1*$^{flox/flox}$; Nestin-Cre brain. RT-qPCR of *Sumf1* gene was performed in whole brain homogenates (full bars) and, as control, in liver homogenates (dashed bars) from *Sumf1*$^{flox/flox}$ (grey bar) and *Sumf1*$^{flox/flox}$; Nestin-Cre (purple bar). (e) Lack of sulfatase activities in *Sumf1*$^{flox/flox}$; Nestin-Cre brain. Enzymatic activities of ArsA, ArsB and ArsC sulfatases were measured in whole brain homogenates (full bars) and liver homogenates (dashed bars) from *Sumf1*$^{flox/flox}$ (grey) and *Sumf1*$^{flox/flox}$; Nestin-Cre (purple). (f) Lysosomal storage in both neurons and astrocytes in *Sumf1*$^{flox/flox}$; Nestin-Cre mouse. Electron micrograph of Sumf1$^{flox/flox}$; Nestin-Cre mouse at 6 months of age showing vacuolization of a neuron (left panel) and an astrocyte (right panel). Enlargements show details of the undigested material contained in the vacuoles. All enzymatic activities are indicated as percentage of activity relative to the control genotype (values represent means of n=3 mice/genotype. *, Student's t test P<0.05, **, Student's t test P<0.01). [Scale bars: 2 μm (c, f).]
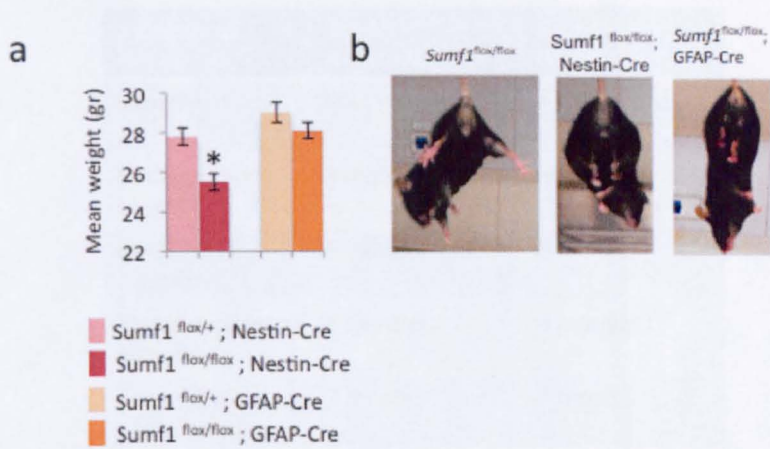
Figure 3.7: *Sumf1*$^{flox/flox}$; Nestin-Cre and *Sumf1*$^{flox/flox}$; GFAP-Cre mouse phenotypes (a) Weight loss in *Sumf1*$^{flox/flox}$; Nestin-Cre. Mean weight values of mice with indicated genotypes at 6 months of age. (Values represent means of n=10 mice for each group. *, Student's t test P<0.05). (b) Abnormal limb-clasping reflexes in both *Sumf1*$^{flox/flox}$; Nestin-Cre and *Sumf1*$^{flox/flox}$; GFAP-Cre mice at 6 months of age.

Symptoms onset	*Sumf1*[flox/flox]; Nestin-Cre	*Sumf1*[flox/flox]; GFAP-Cre
Viability	> 14 months	> 14 months
Reduced body weight	3 months	none
Hindlimb clasping	6 months	6 months
Tremor/epileptic episodes	6 months	6 months
Behavioral abnormalities	7 months	7 months

Table 3.1: Summary of the symptoms onset for *Sumf1*[flox/flox]; Nestin-Cre and *Sumf1*[flox/flox]; GFAP-Cre mice.

3.4 Lysosomal storage in astrocytes causes degeneration of cortical neurons *in vivo*

Regional neurodegeneration was qualitatively evaluated using Nissl staining in sagittal brain sections isolated from $Sumf1^{flox/flox}$; Nestin-Cre, $Sumf1^{flox/flox}$; GFAP-Cre and control mice at 6 months of age (Figure 3.8a). I observed a decreased cellular density in cortical regions in both $Sumf1^{flox/flox}$; Nestin-Cre and $Sumf1^{flox/flox}$; GFAP-Cre mice compared to controls. To perform a quantitative analysis, I undertook a grid-based neuronal count analysis on cortical slices using NeuN immunostaining. At 6 months of age I observed a significant decrease in the number of cortical neurons in $Sumf1^{flox/flox}$; Nestin-Cre compared to control neurons in all the examined layers of the cortex (II to V) (Figure 3.8b,c). Surprisingly, a decreased neuronal number was also observed in the cortex of $Sumf1^{flox/flox}$; GFAP-Cre compared to control mice (Figure 3.8b,c). Interestingly, in $Sumf1^{flox/flox}$; GFAP-Cre this decrease was evident in the more superficial layers (II, III and IV), whereas no significant changes were observed in deeper cortical layers. This phenotype was even more pronounced in 12 month old mice, suggesting a progressive neuronal cell loss (Figure 3.9a,c). These observations suggest that lysosomal storage in cortical

astrocytes is sufficient to trigger degeneration of cortical neurons. I then analyzed Purkinje cells of the cerebellum, as their degeneration is documented in several LSDs (Fischer et al., 1998; Ellinwood et al., 2003; Sleat et al., 2004; Ko et al., 2005; Settembre et al., 2007). Calbindin staining showed a dramatic Purkinje cell loss in $Sumf1^{flox/flox}$; Nestin-Cre mice, whereas no significant differences were found in $Sumf1^{flox/flox}$; GFAP-Cre mice even at 12 months of age (Figure 3.9b, quantification in d), even though there was expression of Cre in the Bergmann glia of these mice (see Figure 3.5c). These data indicated that Purkinje cell degeneration is likely to be cell-autonomous. Interestingly, in younger $Sumf1^{flox/flox}$; Nestin-Cre mice (3 months of age) I observed massive lysosomal vacuolization in Purkinje cells, whereas cortical neurons appear to be less affected (Figure 3.10).
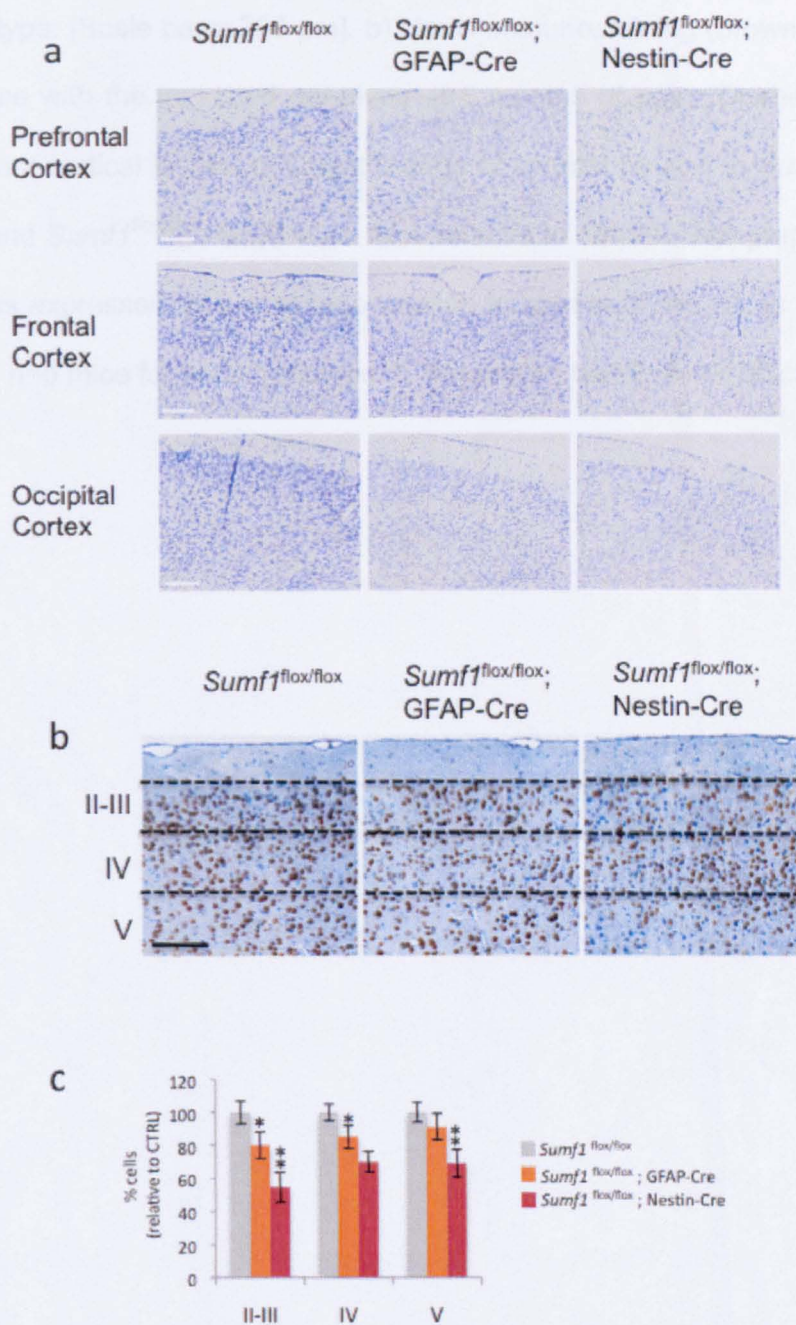
Figure 3.8: Cellular loss in brain cortex of Sumf1^flox/flox; GFAP-Cre and Sumf1^flox/flox; Nestin-Cre mice. a) Nissl staining of brain slices was performed in control (*Sumf1*^flox/flox) mice, *Sumf1*^flox/flox; GFAP-Cre mice and Sumf1^flox/flox; Nestin-

Cre mice at 6 months of age. Different areas of the cortex are shown from each genotype. [Scale bars: 200 µm]. b) NeuN immunostaining (brown) of frontal cortex of mice with the indicated genotype at 6 months of age. Dashed lines mark the different cortical layers. c) Quantification of cortical neuron in $Sumf1^{flox/flox}$; Nestin-Cre and $Sumf1^{flox/flox}$; GFAP-Cre mice relative to control. The graph represents the means expressed as percentage relative to control (three slices were counted for mice; n=5 mice for each genotype. *, Student's t test P<0.05). [Scale bars: 200 µm]

Figure 3.9: Lysosomal storage in astrocytes induces cortical neuronal degeneration. (a) Cortical neuronal loss in $Sumf1^{flox/flox}$; Nestin-Cre and $Sumf1^{flox/flox}$; GFAP-Cre mice. (a) NeuN immunostaining (brown) of frontal cortex of mice with the indicated genotype at 12 months of age. Dashed lines mark the different cortical layers. Boxed areas are enlarged below. (b) Purkinje cell

degeneration in *Sumf1*$^{flox/flox}$; Nestin-Cre mice. Calbindin immunostaining (brown) of Purkinje cells in cerebellar sections obtained from 12 months old mice with indicated genotypes. Boxed area represent an enlargement showing a detail of the Purkinje cell layer. (c,d) Quantification of cortical neuron (c) and of Purkinje cells (d) in *Sumf1*$^{flox/flox}$; Nestin-Cre and *Sumf1*$^{flox/flox}$; GFAP-Cre mice relative to control. The graphs represent the means expressed as percentage relative to control (three slices were counted for mice; n=5 mice for each genotype. *, Student's t test $P<0.05$). [Scale bars: 200 µm]
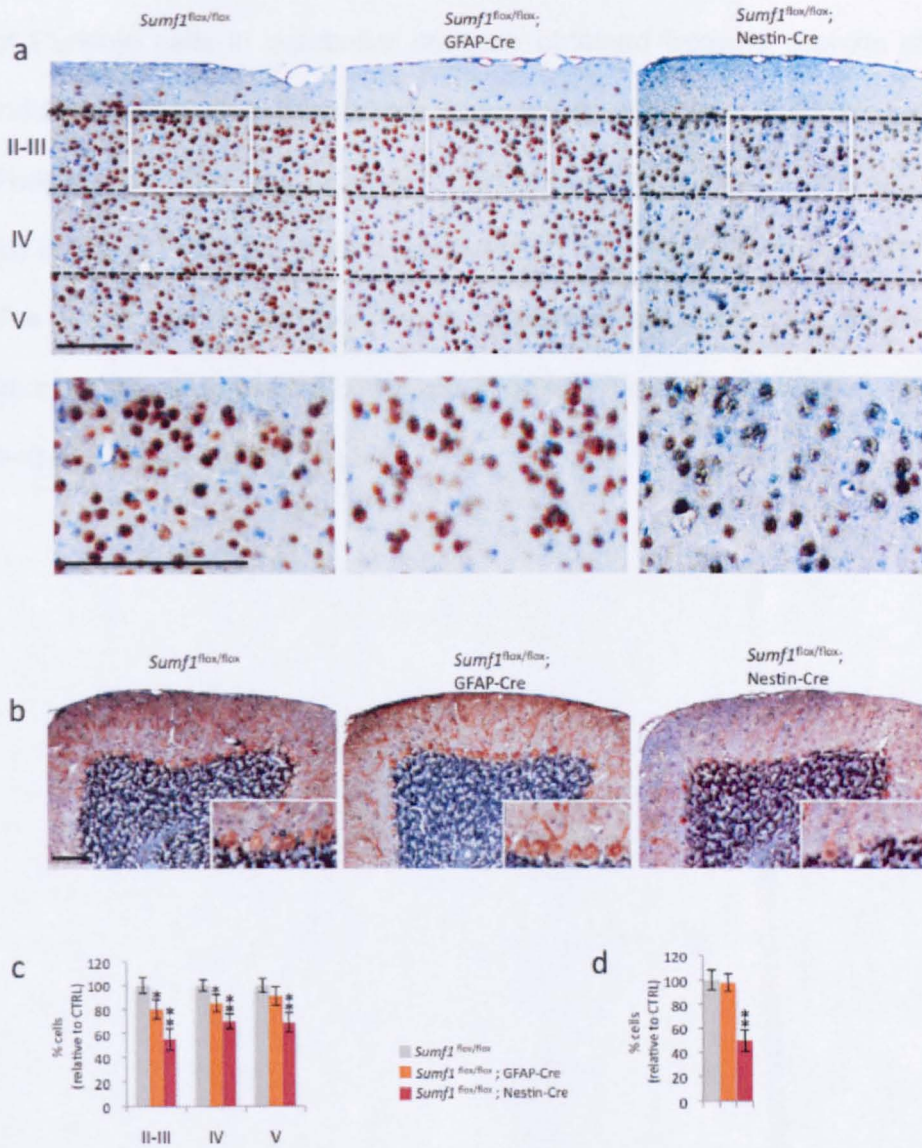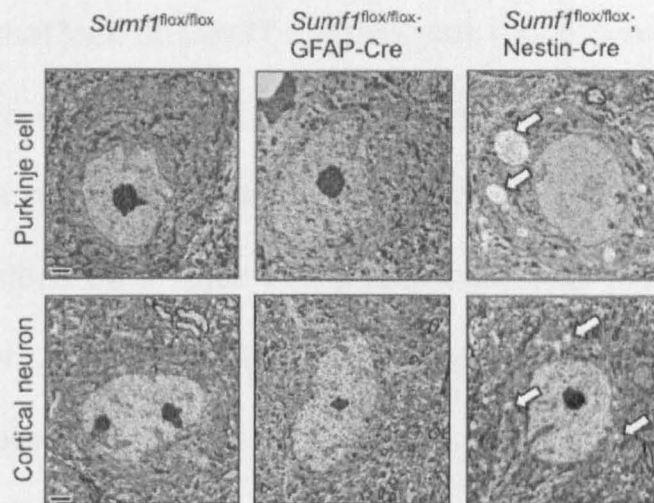
Figure 3.10: Lysosomal storage in cortical neurons and Purkinje cells in 3 months old mice. Electron micrographs showing lysosomal storage in Purkinje cells (top) and cortical neurons (bottom) in $Sumf1^{flox/flox}$; Nestin-Cre (right), in $Sumf1^{flox/flox}$; GFAP-Cre (center) and in control (left). Vacuoles (arrows) are present only in neurons from Sumf1$^{flox/flox}$; Nestin-Cre and the ones in cortical neurons appear fewer and much smaller compared to the ones observed in the Purkinje cells from the same mouse. [Scale bars: 2 µm]

3.5 Lysosomal storage in astrocytes impairs their ability to support cortical neuron survival

To confirm that lack of *Sumf1* in astrocytes can trigger death of cortical neurons, I co-cultured cortical neurons onto a layer of astrocytes. Wild type cortical neurons isolated from embryos at *E*15.5 were plated at similar densities on a layer of cortical astrocytes isolated from either wild type or *Sumf1*$^{-/-}$ newborn mice. After 12 days of culture, the neurons plated on wild type astrocytes formed extensive neuronal networks, whereas the neurons plated on *Sumf1*$^{-/-}$ astrocytes were significantly fewer (63%±8 *vs* ctrl) and appeared less branched (Figure 3.11a).

Excitotoxicity is the pathological process by which neurons are damaged and killed by excessive stimulation by neurotransmitters such as glutamate. Under normal physiological condition, neurotransmitters stimulation is accompanied by the opening of voltage dependent Ca^{2+} channels (VDCC), which cause a small rise in intracellular calcium that can be buffered in the cell. However, neurotransmitters overstimulation induces high calcium conductivity, resulting in high Ca^{2+} loads and, ultimately, mitochondrial damage, apoptosis and cell death (Jaiswal et al., 2009).

As described in Introduction section (1.9.2), astrocytes are deputed to the uptake of glutamate from the neuronal synapses to avoid excessive neuronal stimulation, hence excitotoxicity. Therefore, to evaluate if $Sumf1^{-/-}$ astrocytes were able to protect neurons from excitotoxicity, I challenge neurons with glutamate (0.1mM for 24 hours). This treatment further decreased the survival of the neurons co-cultured with $Sumf1^{-/-}$ astrocytes compared to wild type astrocytes (33%±6 when plated on $Sumf1^{-/-}$ glia vs 65%±10 when plated on wild type glia) (Figure 3.11b). A similar difference was obtained after stimulation with a higher dose of glutamate (0.2mM) (13%±3 when plated on $Sumf1^{-/-}$ glia vs 28%±5 when plated on wild type glia) (Figure 3.11c). To assess whether this effect was indeed specific of an impairment of astrocyte function, I treated the two co-cultures with N-methyl-D-aspartate (NMDA) (0.1mM), which causes neuronal toxicity independently of astrocytes. Indeed, NMDA is a selective agonist for the NMDA receptors that specifically localized on neurons. In this case, treatment with NMDA resulted in comparable cell death (60%±8 when plated on $Sumf1^{-/-}$ glia vs 56%±7 when plated on wild type glia). (Figure 3.11d). Together these data indicate that lysosomal storage

impairs the ability of astrocytes to provide support and protection to cortical neurons.
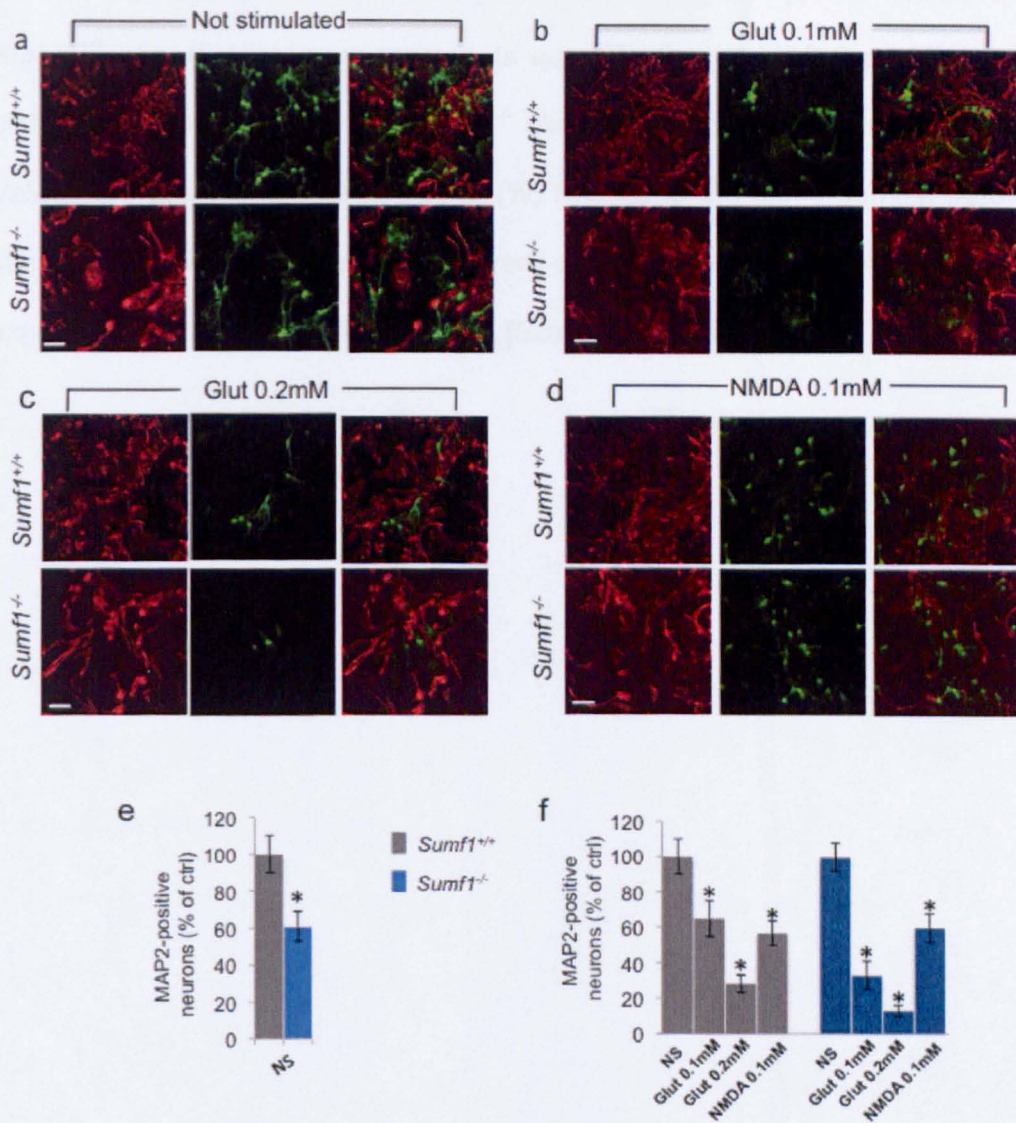
Figure 3.11: Lysosomal storage in astrocytes induces cortical neuron degeneration in an *ex vivo* co-culture assay (a-d) MAP2 (green) and GFAP (red) immunostaining of neurons and astrocytes after 12 days in culture. (a) not stimulated; (b) stimulated with glutamate 0.1mM; (c) stimulated with glutamate 0.2mM; (d) stimulated with NMDA 0.1mM. (e) Histogram represents quantification of MAP2-positive wild type neurons plated on *Sumf1⁻/⁻* glia and left untreated.

Values are expressed as % relative to MAP2-positive wild type neurons plated on *Sumf1*$^{+/+}$ glia. (f) Histogram represents quantification of MAP-2 positive neurons plated on *Sumf1*$^{+/+}$ glia or on *Sumf1*$^{-/-}$ glia and stimulated as indicated for 24h. Values are represented as decrease (%) relative to the same sample before the stimulation. The data (mean ±SEM) were obtained from 3 independent co-culture experiments *, Student's t test P<0.05. [Scale bars: 20 µm]

3.6 Lysosomal storage in neurons elicits neuroinflammation in MSD.

Neuroinflammation is implicated in the progressive nature of several neurodegenerative diseases, and it is described in almost all LSDs with neurological involvement (Wada et al., 2000; Wu et al., 2000; Jeyakumar et al., 2003; Ohmi et al., 2003; Kielar et al., 2007; Settembre et al., 2007; Farfel-Becker et al., 2011). However, it is still unclear whether macrophage and astrocyte activation in LSDs is triggered by their own intracellular storage, or if it represents a response to neuronal damage. To address this, I examined neuroinflammation in my mouse models through F4/80 immunostaing. I observed strong microglial activation in different brain regions of *Sumf1*[flox/flox]; Nestin-Cre mice (Figure 3.12a,b), although in this model the microglia were not subjected to the CRE-mediated *Sumf1* deletion. I did not observe any microglia activation in *Sumf1*[flox/flox]; GFAP-Cre, suggesting that direct neuronal dysfunction triggers microglia activation. Similarly, *Sumf1*[flox/flox]; Nestin-Cre presented severe signs of astroglyosis whereas the *Sumf1*[flox/flox]; GFAP-Cre did not (Figure 3.12c,d), although in both models astrocytes presented lysosomal vacuolization. Furthermore, the mRNA levels of the chemokines *Mip1α*

and *Mip1β* and of the cytokine *TNFα* were significantly upregulated in *Sumf1*^flox/flox; Nestin-Cre mice but not in *Sumf1*^flox/flox; GFAP-Cre mice compared to control mice (Figure 3.12e). These observations clearly indicate that lysosomal storage in neurons, rather than in astrocytes or microglia, triggers neuroinflammation in LSDs.
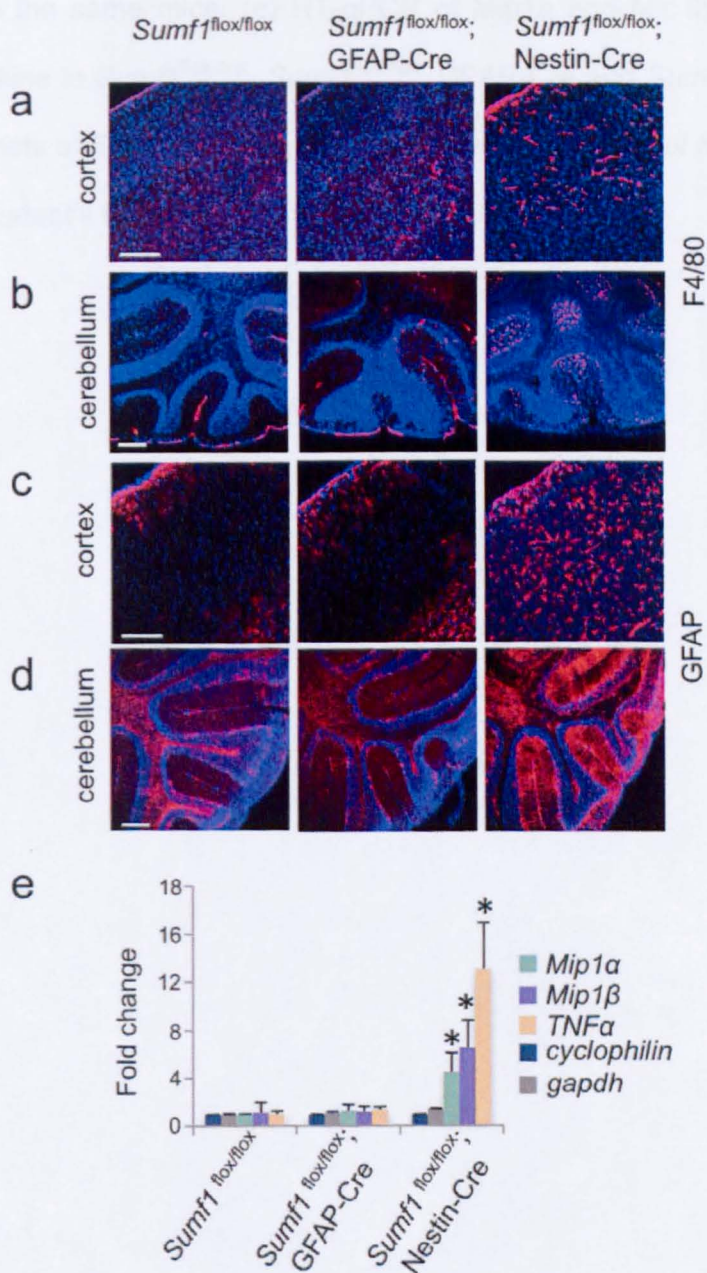
Figure 3.12: **Neuroinflammation in Sumf1**^{flox/flox}**; Nestin-Cre but not in Sumf1**^{flox/flox}**; GFAP-Cre mouse brain.** (a,b) F4/80 immunostaining in cortical (a) and cerebellar (b) sections isolated from 6 months old mice with indicated genotype. (c,d) GFAP immunostaining of cortical (c) and cerebellar (d) sections

from the same mice. (e) RT-qPCR of Mip1a and Mip1b chemokines and TNFa cytokine in *Sumf1*^{flox/flox}, *Sumf1*^{flox/flox}; GFAP-Cre and *Sumf1*^{flox/flox}; Nestin-Cre brain extracts at 6 months of age (values represent means of n=3 mice for each group. *, Student's t test $P<0.05$). [Scale bars: 200 μm (a-d).]

3.7 Astrocyte dysfunction contributes to MSD behavioural abnormalities

To study the neurological phenotype in MSD without the influence of peripheral organ dysfunction and to understand the contribution of astrocytes, I performed a panel of behavioural tests in both *Sumf1*$^{flox/flox}$; Nestin-Cre and *Sumf1*$^{flox/flox}$; GFAP-Cre and their littermate controls. At 7 months of age, mice from both genotypes showed a statistically significant impairment in motor performance as assessed by decreased latency to fall in the rotarod test and increased number of footfalls in the parallel-rod test (Figure 3.13a,b). However, *Sumf1*$^{flox/flox}$; Nestin-Cre mice were unable to improve their performance on the rotarod after several trials, whereas the *Sumf1*$^{flox/flox}$; GFAP-Cre mice showed signs of improvement (Figure 3.13a). The *Sumf1*$^{flox/flox}$; Nestin-Cre also presented a specific hyperactive behaviour as demonstrated by both Open Field and Light/Dark tests (Figure 3.13c-h) whereas the *Sumf1*$^{flox/flox}$; GFAP-Cre mice were significantly hypoactive and more anxious compared with control mice since they spent less time in the light and had a reduced number of transits in light/dark test and horizontal beam breaks (Figure

3.13g-i). The behavioural phenotype observed in $Sumf1^{flox/flox}$; Nestin-Cre and in $Sumf1^{flox/flox}$; GFAP-Cre mice are summarized in Table 3.2.

Therefore, although concomitant storage in neurons and glia causes a more severe phenotype, the lysosomal dysfunction in astrocytes only is sufficient to cause neurological impairment.
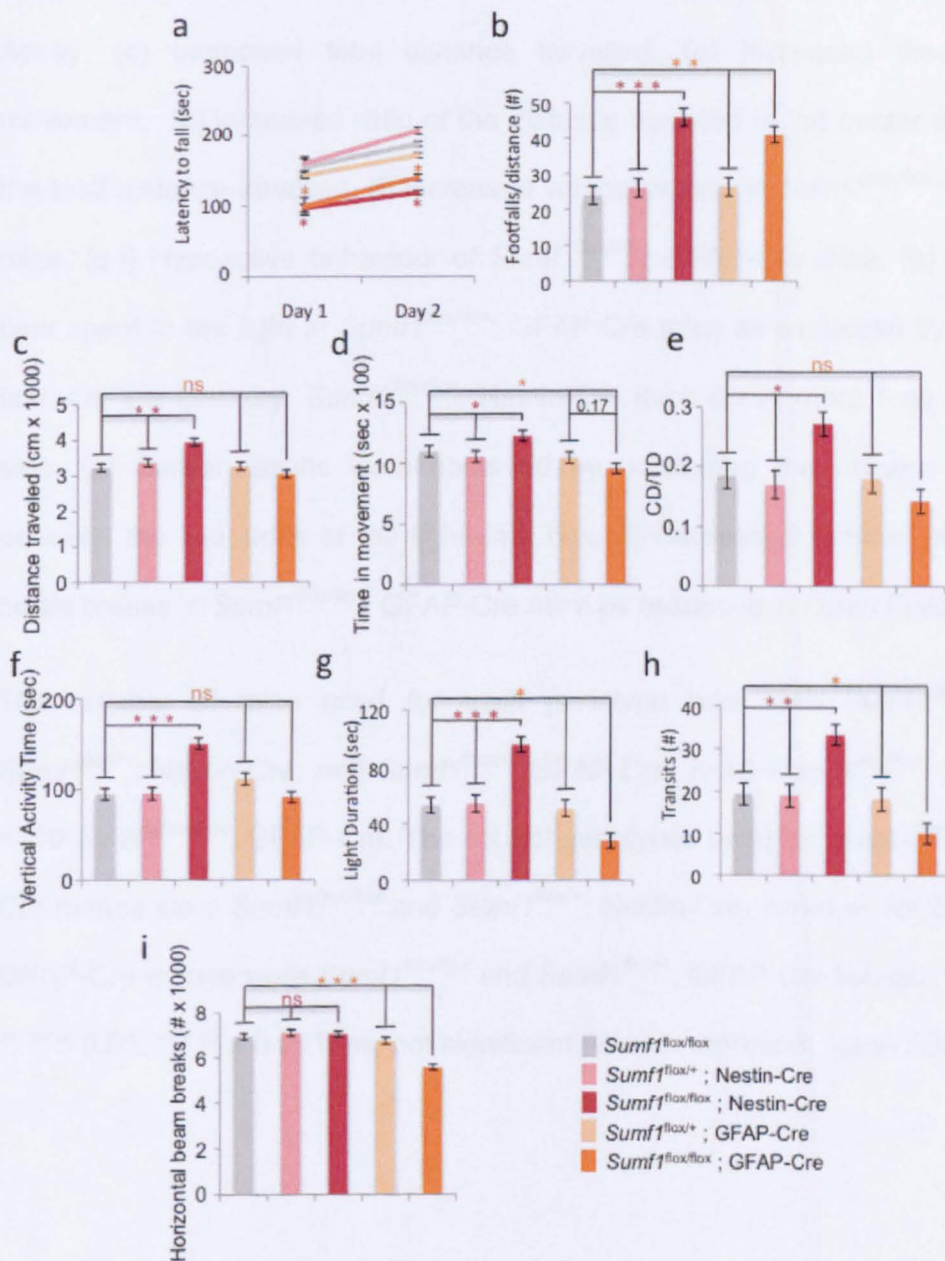
Figure 3.13: Astrocyte dysfunction contributes to MSD neurological impairment (a) Rotarod Test: *Sumf1*^flox/flox^; Nestin-Cre and *Sumf1*^flox/flox^; GFAP-Cre mice showed decreased latency to fall. (b) Parallel rod test: Increased number of footfalls for both *Sumf1*^flox/flox^; Nestin-Cre and *Sumf1*^flox/flox^; GFAP-Cre mice. (c-f)

Hyperactive behavior of $Sumf1^{flox/flox}$; Nestin-Cre mice as assessed in Open Field Assay. (c) Increased total distance travelled, (d) increased time spent in movement, (e) increased ratio of the distance travelled in the center with respect the total distance travelled, (f) increased vertical activity in $Sumf1^{flox/flox}$; Nestin-Cre mice. (g-i) Hypoactive behaviour of $Sumf1^{flox/flox}$; GFAP-Cre mice. (g) Decreased time spent in the light in $Sumf1^{flox/flox}$; GFAP-Cre mice as assessed by Light/Dark test. On the contrary, $Sumf1^{flox/flox}$; Nestin-Cre mice spent more time in the light side. (h) Similar results were observed by measuring the number of transits between the two sides of the light-dark box. (i) Decreased number of horizontal beam breaks in $Sumf1^{flox/flox}$; GFAP-Cre mice as assessed in Open Field.

The number of mice used for each genotype was: n=9 $Sumf1^{flox/flox}$; n=8 $Sumf1^{flox/+}$; Nestin-Cre; n=8 $Sumf1^{flox/+}$; GFAP-Cre; n=10 $Sumf1^{flox/flox}$; Nestin-Cre; n=10 $Sumf1^{flox/flox}$; GFAP-Cre. The control genotypes used for $Sumf1^{flox/flox}$; Nestin-Cre mouse were $Sumf1^{flox/flox}$ and $Sumf1^{flox/+}$; Nestin-Cre, whereas for $Sumf1^{flox/flox}$; GFAP-Cre mouse were $Sumf1^{flox/flox}$ and $Sumf1^{flox/+}$; GFAP-Cre mouse. *, P ≤ 0.05; ** P ≤ 0.01; *** P ≤ 0.001. ns, not significant. Values represent mean ±SEM.

Neurological features	$Sumf1^{flox/flox}$; Nestin-Cre	$Sumf1^{flox/flox}$; GFAP-Cre
Hyperactivity	×	
Altered weight	×	
Hindlimb clasping	×	×
Motor incoordination	×	×
Motor learning	×	
Hypoactivity		×
Anxiety		×

Table 3.2: Summary of the neurological features found in $Sumf1^{flox/flox}$; Nestin-Cre and $Sumf1^{flox/flox}$; GFAP-Cre mice. Comparison between the data obtained from the analysis of the two mouse models shows distinct behavioural phenotypes. "X" indicates the presence of the alterations in the specific LSD neurological feature.

Discussion

Astrocytes are the main neural cell type responsible for the maintenance of brain homeostasis. Their processes form extensive networks, which modulate neuronal activity through the expression of various receptors for neurotransmitters, several transporters, cytokines and growth factors. Indeed, they play critical roles in neurotransmitter trafficking and recycling, nutrient and ion metabolism, and protect against oxidative stress (Belanger and Magistretti, 2009). Consistent with such a variety of fundamental functions exerted by astrocytes to support neurons, astrocyte impairment has been found to contribute to neuronal dysfunction in several neurodegenerative diseases.

In Amyotrophic lateral sclerosis (ALS), deletion of the mutant form of superoxide dismutase in astrocytes only, delayed microglial activation and sharply slowed later disease progression of the mouse model of ALS (Yamanaka et al., 2008).

Moreover, reactive astrocytes are observed in close association with Aβ plaques in the brains of Alzheimer disease patients (Nagele et al., 2004) and have been shown to be capable of internalizing and degrading Aβ peptides (Nagele et al., 2003). Consistently, when exogenous astrocytes were transplanted into the brain of Aβ plaque-bearing transgenic mice, they migrated towards Aβ deposits and internalized Aβ-positive material (Pihlaja et al., 2008).

Furthermore, a mouse model of Huntington disease expressing the mutant form of huntingtin in astrocytes only, presented an age-dependent neurological phenotype: body weight loss, motor function deficits, and untimely death (Bradford et al., 2009). Finally, it was recently shown that in a mouse model of Rett's syndrome, re-expression of the depleted gene (*MECP2*) in astrocytes only, significantly improved locomotion and anxiety levels, restored neuronal abnormalities, restored respiratory abnormalities to a normal pattern, and greatly prolonged lifespan compared control mice (Lioy et al., 2011).

The contribution of astrocyte impairment to neuronal dysfunction in human degenerative diseases could actually be even more important than can be addressed using mouse models. There has been a dramatic increase in the number and complexity of astroglia during the course of evolution: a steady increase of the astrocyte-to-neuron ratio, going from about 1/6 in nematodes to 1/3 in rodents, and reaching up to 1.65 astrocytes per neuron in the human cortex (Sherwood et al., 2006). Importantly, more than simply outnumbering their rodent counterparts, human astrocytes are also strikingly more complex, both morphologically and functionally. In comparison, human neocortical

astrocytes are 2.5 times larger, extend 10 times more processes, and display unique microanatomical features. In addition, they generate more robust intracellular Ca^{2+} responses to neurotransmitter receptor agonists and display a 4-fold increase in Ca^{2+} wave velocity (Oberheim et al., 2009). This points to a role for astrocytes in the evolution of uniquely human traits such as cognition and further suggests that astrocytes likely play roles in neurological diseases.

Neurodegeneration is one of the most common and prominent features in LSDs. Neuropathological symptoms include developmental delay, abnormal ocular movements, ataxia, seizures, movement disorders, spasticity, visual loss and psychiatric disease (psychosis, depression and dementia)(Platt FM, 2004). However, very little is known about the role of astrocytes in LSDs neuropathogenesis.

During my PhD I studied a severe type of LSD known as Multiple Sulfatase Deficiency. To analyze the contribution of astrocytes to the neurological phenotype of MSD, I generated a conditional knockout mouse line of the *Sumf1* gene and crossed it with a transgenic mouse line expressing the Cre recombinase gene under the control of GFAP promoter, to delete *Sumf1* only in astrocytes. I observed that removing *Sumf1* in astrocytes caused lysosomal/autophagic dysfunction and in

turn led to the accumulation of toxic substrates in their cytoplasm. Based on my results, I cannot conclude at which steps the lysosomal storage impairs the autophagic process. However, the presence of large autolysosomes in the cytoplasm of $Sumf1^{-/-}$ astrocytes supports a model in which the autophagic block occurs at level of intralysosomal degradation of autophagic substrates. Further studies will be required to address more in detail this aspect.

I found both *in vivo* and *in vitro* that astrocytes deprived of *Sumf1* gene directly contributed to neurodegeneration since they lost their ability to support neuronal survival and function. This supportive function appeared to be particularly important for cortical neuron survival, although I cannot formally exclude that also other neuronal populations were affected in $Sumf1^{flox/flox}$; GFAP-Cre mice.

Recent studies performed on a model of LSD, Niemann-Pick type C disease, showed that selective deletion of *Npc1* gene only in astrocytes did not induce neurodegeneration, and indeed this disease is largely caused by a cell-autonomous Purkinje cell degeneration (Elrick et al., 2010; Yu et al., 2011). Consistent with this observation, I found that while lysosomal dysfunction in astrocytes may represent a significant determinant for cortical neuronal degeneration, a cell autonomous pathway accounted for Purkinje cell death, since these

neurons only degenerated in the *Sumf1*^{flox/flox}; Nestin-Cre mice. In support of this model, in 3 months old *Sumf1*^{flox/flox}; Nestin-Cre mice I observed a massive lysosomal vacuolization in Purkinje cells whereas it was barely detectable in cortical neurons (Figure 3.10). This difference may be due to a higher glycosaminoglycan metabolism in Purkinje cells compared to cortical neurons. Together these data indicated that, in LSDs, neurodegeneration involves both cell autonomous and non-autonomous pathways.

Lysosomal enzymes are either targeted to the lysosome or secreted in a mannose-6-phosphate receptor dependent fashion (Ni et al., 2006). Secreted enzymes can be taken up by the surrounding cells or even by distant cells through the circulation. This secretion/uptake mechanism most likely account for the milder cellular phenotype observed in *Sumf1*^{flox/flox}; Nestin-Cre compared to the one found in *Sumf1*^{-/-} mice (compare vacuolization in Figure 3.6f with the one observed in Figure 3.2a). In *Sumf1*^{flox/flox}; Nestin-Cre sulfatases may be secreted by non-recombined cells such as microglia and blood vessel cells and taken up by neurons and astrocytes. However, my data indicate that uptake of enzymes from healthy cell types is not able to compensate for the genetic defect. Indeed, even if for some LSDs hematopoietic stem cell transplantation (HSCT) has demonstrated some efficacy proving that

donor-derived macrophages and microglia can progressively become a stable source of endogenous enzyme in the central nervous system, for many others this approach has been unsatisfactory (Orchard et al., 2007). Currently, new promising therapies combine gene therapy and HSCT to obtain hematopoietic donor cells that express supra-physiological levels of the absent enzyme resulting in increased levels of enzyme secretion (Biffi et al., 2004).

Considering that astrocytes make up as much as 50% of the brain's volume (Benarroch, 2005), the observation that astrocyte dysfunction significantly contributes to neurodegeneration in MSD may suggest also a new alternative therapeutic approach for the treatment of neurological impairment in LSDs.

In the recent years neural precursor cell (NPC) transplantation has been described as a strategy for slowing neurodegenerative disease progression because engrafted cells have the potential of replacing lost or dysfunctional neurons and glia. However, this is a challenging strategy for neurodegenerative diseases because of problems related to neuronal differentiation and to the establishment of appropriate circuitry with host neurons (Le Belle and Svendsen, 2002). In addition to NPCs, there is an increasing literature that implicates a direct glial

cell-mediated neuroprotective effect in models of acute and progressive neuronal injury through modification of a hostile endogenous astroglial environment in the context of noncell-autonomous neurodegeneration. Transplantation of glia-restricted precursors extended survival and disease duration, attenuated motor neuron loss, and slowed declines in fore-limb motor and respiratory physiological function in a rat model of ALS (Lepore et al., 2008). Moreover, direct astrocyte implantation reduced cortical neuron degeneration in a transgenic mouse of a tauopathy (Hampton et al., 2010). Similarly, this approach could represent an intriguing therapeutic strategy to treat some aspects of the neurological manifestation of LSDs.

Because in LSDs with neurological involvement all the cell types of the brain are affected by the lysosomal storage, the activation of the inflammatory system could be either the consequence of the intracellular storage in astrocytes and microglia or the secondary effect of neuronal damage. Neuroinflammation has been proposed to induce oxidative stress, excitotoxicity and metabolic failure in neurodegenerative diseases. In this scenario the suffering reactive astrocytes and microglia would exacerbate neuronal deterioration at a

later stage of disease progression (Allan and Rothwell, 2003; Sofroniew, 2005; Farina et al., 2007). I observed signs of neuroinflammation characterized by microglial activation and astrogliosis only in $Sumf1^{flox/flox}$; Nestin-Cre. This observation suggests at least two important conclusions: 1) microglial activation and astrogliosis are triggered by neuronal dysfunction probably as an attempt to clear dying cells and 2) astrogliosis does not represent the main mechanism through which astrocytes contribute to the neurodegeneration in LSDs, since no signs of astrogliosis were observed in $Sumf1^{flox/flox}$; GFAP-Cre mice. Most likely, aberrant lysosomal storage in astrocytes hampers more fundamental and supportive functions needed for neuronal survival.

Exhaustive descriptions of the neurological phenotype of the MSD mouse model had not been possible in previous studies because of the early lethality caused by the complex systemic phenotype (Settembre et al., 2007; Settembre et al., 2008a). The generation of the conditional $Sumf1$ mouse line allowed us to overcome this limitation. I observed distinct behavioural phenotypes in $Sumf1^{flox/flox}$; Nestin-Cre and $Sumf1^{flox/flox}$; GFAP-Cre: while they both showed significant impairment in motor performance, the deletion of $Sumf1$ gene only in astrocytes

caused hypoactivity and anxiety-like behaviour, whereas its lack in both neurons and glia was responsible for hyperactivity and reduced learning ability. Interestingly, these neurological symptoms represent common features observed in different phases of disease manifestations in LSDs: fear and anxiety are generally reported as early symptoms, whereas hyperactivity, learning difficulties and progressive neurodegeneration occur at a later stage of the disease (Staretz-Chacham et al., 2010) .

Thus, my data suggest that the progressive neurological deterioration found in MSD patients could result from at least two independent insults to neurons: one non-autonomous caused by astrocyte dysfunction and another, more severe, cell autonomous insult due to the lysosomal engulfment and dysfunction.

References

Abe T, Norton WT. 1974. The characterization of sphingolipids from neurons and astroglia of immature rat brain. J Neurochem 23:1025-1036.

Allan SM, Rothwell NJ. 2003. Inflammation in central nervous system injury. Philos Trans R Soc Lond B Biol Sci 358:1669-1677.

Bak LK, Schousboe A, Waagepetersen HS. 2006. The glutamate/GABA-glutamine cycle: aspects of transport, neurotransmitter homeostasis and ammonia transfer. J Neurochem 98:641-653.

Ballabio A, Gieselmann V. 2009. Lysosomal disorders: from storage to cellular damage. Biochim Biophys Acta 1793:684-696.

Ballabio A SL. 2001. Steroid sulfatase deficiency and X-linked ichthyosis. In: Scriver S, editor. pp 4241–4262.

Belanger M, Magistretti PJ. 2009. The role of astroglia in neuroprotection. Dialogues Clin Neurosci 11:281-295.

Benarroch EE. 2005. Neuron-astrocyte interactions: partnership for normal function and disease in the central nervous system. Mayo Clin Proc 80:1326-1338.

Benjamins JA, Guarnieri M, Miller K, Sonneborn M, McKhann GM. 1974. Sulphatide synthesis in isolated oligodendroglial and neuronal cells. J Neurochem 23:751-757.

Biffi A, De Palma M, Quattrini A, Del Carro U, Amadio S, Visigalli I, Sessa M, Fasano S, Brambilla R, Marchesini S, Bordignon C, Naldini L. 2004. Correction of metachromatic leukodystrophy in the mouse model by transplantation of genetically modified hematopoietic stem cells. J Clin Invest 113:1118-1129.

Bignami A, Eng LF, Dahl D, Uyeda CT. 1972. Localization of the glial fibrillary acidic protein in astrocytes by immunofluorescence. Brain Res 43:429-435.

Bjorkoy G, Lamark T, Brech A, Outzen H, Perander M, Overvatn A, Stenmark H, Johansen T. 2005. p62/SQSTM1 forms protein aggregates degraded by autophagy and has a protective effect on huntingtin-induced cell death. J Cell Biol 171:603-614.

Bradford J, Shin JY, Roberts M, Wang CE, Li XJ, Li S. 2009. Expression of mutant huntingtin in mouse brain astrocytes causes age-dependent neurological symptoms. Proc Natl Acad Sci U S A 106:22480-22485.

Brenner M, Kisseberth WC, Su Y, Besnard F, Messing A. 1994. GFAP promoter directs astrocyte-specific expression in transgenic mice. J Neurosci 14:1030-1037.

Brown AM, Ransom BR. 2007. Astrocyte glycogen and brain energy metabolism. Glia 55:1263-1271.

Bulow HE, Hobert O. 2006. The molecular diversity of glycosaminoglycans shapes animal development. Annu Rev Cell Dev Biol 22:375-407.

Chen Y, Vartiainen NE, Ying W, Chan PH, Koistinaho J, Swanson RA. 2001. Astrocytes protect neurons from nitric oxide toxicity by a glutathione-dependent mechanism. J Neurochem 77:1601-1610.

Clements JD, Lester RA, Tong G, Jahr CE, Westbrook GL. 1992. The time course of glutamate in the synaptic cleft. Science 258:1498-1501.

Colton CA. 2009. Heterogeneity of microglial activation in the innate immune response in the brain. J Neuroimmune Pharmacol 4:399-418.

Copeland NG, Jenkins NA, Court DL. 2001. Recombineering: a powerful new tool for mouse functional genomics. Nat Rev Genet 2:769-779.

Cosma MP, Pepe S, Annunziata I, Newbold RF, Grompe M, Parenti G, Ballabio A. 2003. The multiple sulfatase deficiency gene encodes an essential and limiting factor for the activity of sulfatases. Cell 113:445-456.

Cosma MP, Pepe S, Parenti G, Settembre C, Annunziata I, Wade-Martins R, Di Domenico C, Di Natale P, Mankad A, Cox B, Uziel G, Mancini GM, Zammarchi E, Donati MA, Kleijer WJ, Filocamo M, Carrozzo R, Carella M, Ballabio A. 2004. Molecular and functional analysis of SUMF1 mutations in multiple sulfatase deficiency. Hum Mutat 23:576-581.

Cox TM, Cachon-Gonzalez MB. 2012. The cellular pathology of lysosomal diseases. J Pathol 226:241-254.

Crack PJ, Bray PJ. 2007. Toll-like receptors in the brain and their potential roles in neuropathology. Immunol Cell Biol 85:476-480.

Danbolt NC. 2001. Glutamate uptake. Prog Neurobiol 65:1-105.

Deitmer JW. 2002. A role for CO_2 and bicarbonate transporters in metabolic exchanges in the brain. J Neurochem 80:721-726.

Dhoot GK, Gustafsson MK, Ai X, Sun W, Standiford DM, Emerson CP, Jr. 2001. Regulation of Wnt signaling and embryo patterning by an extracellular sulfatase. Science 293:1663-1666.

Dierks T, Dickmanns A, Preusser-Kunze A, Schmidt B, Mariappan M, von Figura K, Ficner R, Rudolph MG. 2005. Molecular basis for multiple sulfatase deficiency

and mechanism for formylglycine generation of the human formylglycine-generating enzyme. Cell 121:541-552.

Dierks T, Schmidt B, Borissenko LV, Peng J, Preusser A, Mariappan M, von Figura K. 2003. Multiple sulfatase deficiency is caused by mutations in the gene encoding the human C(alpha)-formylglycine generating enzyme. Cell 113:435-444.

Diez-Roux G, Ballabio A. 2005. Sulfatases and human disease. Annu Rev Genomics Hum Genet 6:355-379.

Dringen R, Hirrlinger J. 2003. Glutathione pathways in the brain. Biol Chem 384:505-516.

Ellinwood NM, Wang P, Skeen T, Sharp NJ, Cesta M, Decker S, Edwards NJ, Bublot I, Thompson JN, Bush W, Hardam E, Haskins ME, Giger U. 2003. A model of mucopolysaccharidosis IIIB (Sanfilippo syndrome type IIIB): N-acetyl-alpha-D-glucosaminidase deficiency in Schipperke dogs. J Inherit Metab Dis 26:489-504.

Elrick MJ, Pacheco CD, Yu T, Dadgar N, Shakkottai VG, Ware C, Paulson HL, Lieberman AP. 2010. Conditional Niemann-Pick C mice demonstrate cell autonomous Purkinje cell neurodegeneration. Hum Mol Genet 19:837-847.

Eric R. Kandel JHS, Thomas M. Jessel. 2000. Principles of neural science. Mc Graw Hill.

Farfel-Becker T, Vitner EB, Pressey SN, Eilam R, Cooper JD, Futerman AH. 2011. Spatial and temporal correlation between neuron loss and neuroinflammation in a mouse model of neuronopathic Gaucher disease. Hum Mol Genet 20:1375-1386.

Farina C, Aloisi F, Meinl E. 2007. Astrocytes are active players in cerebral innate immunity. Trends Immunol 28:138-145.

Fischer A, Carmichael KP, Munnell JF, Jhabvala P, Thompson JN, Matalon R, Jezyk PF, Wang P, Giger U. 1998. Sulfamidase deficiency in a family of Dachshunds: a canine model of mucopolysaccharidosis IIIA (Sanfilippo A). Pediatr Res 44:74-82.

Fraldi A, Annunziata F, Lombardi A, Kaiser HJ, Medina DL, Spampanato C, Fedele AO, Polishchuk R, Sorrentino NC, Simons K, Ballabio A. 2010. Lysosomal fusion and SNARE function are impaired by cholesterol accumulation in lysosomal storage disorders. EMBO J 29:3607-3620.

France JT, Liggins GC. 1969. Placental sulfatase deficiency. J Clin Endocrinol Metab 29:138-141.

France JT, Seddon RJ, Liggins GC. 1973. A study of pregnancy with low estrogen production due to placental sulfatase deficiency. J Clin Endocrinol Metab 36:1-9.

Franco B, Meroni G, Parenti G, Levilliers J, Bernard L, Gebbia M, Cox L, Maroteaux P, Sheffield L, Rappold GA, Andria G, Petit C, Ballabio A. 1995. A cluster of sulfatase genes on Xp22.3: mutations in chondrodysplasia punctata (CDPX) and implications for warfarin embryopathy. Cell 81:15-25.

Freeman MR. 2010. Specification and morphogenesis of astrocytes. Science 330:774-778.

Futerman AH, van Meer G. 2004. The cell biology of lysosomal storage disorders. Nat Rev Mol Cell Biol 5:554-565.

Halassa MM, Fellin T, Haydon PG. 2007. The tripartite synapse: roles for gliotransmission in health and disease. Trends Mol Med 13:54-63.

Hampton DW, Webber DJ, Bilican B, Goedert M, Spillantini MG, Chandran S. 2010. Cell-mediated neuroprotection in a mouse model of human tauopathy. J Neurosci 30:9973-9983.

Hanson SR, Best MD, Wong CH. 2004. Sulfatases: structure, mechanism, biological activity, inhibition, and synthetic utility. Angew Chem Int Ed Engl 43:5736-5763.

Hara T, Nakamura K, Matsui M, Yamamoto A, Nakahara Y, Suzuki-Migishima R, Yokoyama M, Mishima K, Saito I, Okano H, Mizushima N. 2006. Suppression of

basal autophagy in neural cells causes neurodegenerative disease in mice. Nature 441:885-889.

Hopwood JJ BA. 2001. Multiple sulfatase deficiency and the nature of the sulfatase family. In: CR Scriver AB, WS Sly, editor. The Metabolic and Molecular Basis of Inherited Disease. New York: McGraw-Hill. pp 3725–3732.

Izant JG, McIntosh JR. 1980. Microtubule-associated proteins: a monoclonal antibody to MAP2 binds to differentiated neurons. Proc Natl Acad Sci U S A 77:4741-4745.

Jaiswal MK, Zech WD, Goos M, Leutbecher C, Ferri A, Zippelius A, Carri MT, Nau R, Keller BU. 2009. Impairment of mitochondrial calcium handling in a mtSOD1 cell culture model of motoneuron disease. BMC Neurosci 10:64.

Jeyakumar M, Thomas R, Elliot-Smith E, Smith DA, van der Spoel AC, d'Azzo A, Perry VH, Butters TD, Dwek RA, Platt FM. 2003. Central nervous system inflammation is a hallmark of pathogenesis in mouse models of GM1 and GM2 gangliosidosis. Brain 126:974-987.

Kabeya Y, Mizushima N, Ueno T, Yamamoto A, Kirisako T, Noda T, Kominami E, Ohsumi Y, Yoshimori T. 2000. LC3, a mammalian homologue of yeast Apg8p, is localized in autophagosome membranes after processing. EMBO J 19:5720-5728.

Kielar C, Maddox L, Bible E, Pontikis CC, Macauley SL, Griffey MA, Wong M, Sands MS, Cooper JD. 2007. Successive neuron loss in the thalamus and cortex in a mouse model of infantile neuronal ceroid lipofuscinosis. Neurobiol Dis 25:150-162.

Kim KK, Adelstein RS, Kawamoto S. 2009. Identification of neuronal nuclei (NeuN) as Fox-3, a new member of the Fox-1 gene family of splicing factors. J Biol Chem 284:31052-31061.

Ko DC, Milenkovic L, Beier SM, Manuel H, Buchanan J, Scott MP. 2005. Cell-autonomous death of cerebellar purkinje neurons with autophagy in Niemann-Pick type C disease. PLoS Genet 1:81-95.

Kofuji P, Newman EA. 2004. Potassium buffering in the central nervous system. Neuroscience 129:1045-1056.

Komatsu M, Waguri S, Chiba T, Murata S, Iwata J, Tanida I, Ueno T, Koike M, Uchiyama Y, Kominami E, Tanaka K. 2006. Loss of autophagy in the central nervous system causes neurodegeneration in mice. Nature 441:880-884.

Kuma A, Mizushima N. 2008. Chromosomal mapping of the GFP-LC3 transgene in GFP-LC3 mice. Autophagy 4:61-62.

Le Belle JE, Svendsen CN. 2002. Stem cells for neurodegenerative disorders: where can we go from here? BioDrugs 16:389-401.

Lepore AC, Rauck B, Dejea C, Pardo AC, Rao MS, Rothstein JD, Maragakis NJ. 2008. Focal transplantation-based astrocyte replacement is neuroprotective in a model of motor neuron disease. Nat Neurosci 11:1294-1301.

Lieberman AP, Puertollano R, Raben N, Slaugenhaupt S, Walkley SU, Ballabio A. 2012. Autophagy in lysosomal storage disorders. Autophagy 8:719-730.

Lioy DT, Garg SK, Monaghan CE, Raber J, Foust KD, Kaspar BK, Hirrlinger PG, Kirchhoff F, Bissonnette JM, Ballas N, Mandel G. 2011. A role for glia in the progression of Rett's syndrome. Nature 475:497-500.

Maragakis NJ, Rothstein JD. 2006. Mechanisms of Disease: astrocytes in neurodegenerative disease. Nat Clin Pract Neurol 2:679-689.

Marinkovic-Ilsen A, Koppe JG, Jobsis AC, de Groot WP. 1978. Enzymatic basis of typical X-linked ichthyosis. Lancet 2:1097.

McGeer PL, McGeer EG. 2002. Inflammatory processes in amyotrophic lateral sclerosis. Muscle Nerve 26:459-470.

McKenna MC. 2007. The glutamate-glutamine cycle is not stoichiometric: fates of glutamate in brain. J Neurosci Res 85:3347-3358.

Mizushima N, Yoshimori T, Levine B. 2010. Methods in mammalian autophagy research. Cell 140:313-326.

Molofsky AV, Krenick R, Ullian E, Tsai HH, Deneen B, Richardson WD, Barres BA, Rowitch DH. 2012. Astrocytes and disease: a neurodevelopmental perspective. Genes Dev 26:891-907.

Nagele RG, D'Andrea MR, Lee H, Venkataraman V, Wang HY. 2003. Astrocytes accumulate A beta 42 and give rise to astrocytic amyloid plaques in Alzheimer disease brains. Brain Res 971:197-209.

Nagele RG, Wegiel J, Venkataraman V, Imaki H, Wang KC. 2004. Contribution of glial cells to the development of amyloid plaques in Alzheimer's disease. Neurobiol Aging 25:663-674.

Neufeld EF MJ. 2001a. The mucopolysaccharidoses. In: CR Scriver AB, WS Sly, D, Valle, editors. In The Metabolic and Molecular Basis of Inherited Diseaseed. New York: McGraw-Hill. pp 3421-3452.

Neufeld EF MJ. 2001b. The mucopolysaccharidoses. In: The Metabolic and Molecular Basis of Inherited Disease eCS, AL Beaudet, WS Sly, D Valle, editor.New York: McGraw-Hill. pp 3421–3452.

Ni X, Canuel M, Morales CR. 2006. The sorting and trafficking of lysosomal proteins. Histol Histopathol 21:899-913.

Norenberg MD, Martinez-Hernandez A. 1979. Fine structural localization of glutamine synthetase in astrocytes of rat brain. Brain Res 161:303-310.

Obara M, Szeliga M, Albrecht J. 2008. Regulation of pH in the mammalian central nervous system under normal and pathological conditions: facts and hypotheses. Neurochem Int 52:905-919.

Oberheim NA, Takano T, Han X, He W, Lin JH, Wang F, Xu Q, Wyatt JD, Pilcher W, Ojemann JG, Ransom BR, Goldman SA, Nedergaard M. 2009. Uniquely hominid features of adult human astrocytes. J Neurosci 29:3276-3287.

Ohmi K, Greenberg DS, Rajavel KS, Ryazantsev S, Li HH, Neufeld EF. 2003. Activated microglia in cortex of mouse models of mucopolysaccharidoses I and IIIB. Proc Natl Acad Sci U S A 100:1902-1907.

Orchard PJ, Blazar BR, Wagner J, Charnas L, Krivit W, Tolar J. 2007. Hematopoietic cell therapy for metabolic disease. J Pediatr 151:340-346.

Parenti G, Meroni G, Ballabio A. 1997. The sulfatase gene family. Curr Opin Genet Dev 7:386-391.

Patricia C. Cross KLM. 1993. Cell and Tissue Ultrastructure: A Functional Perspective.

Peghini P, Janzen J, Stoffel W. 1997. Glutamate transporter EAAC-1-deficient mice develop dicarboxylic aminoaciduria and behavioral abnormalities but no neurodegeneration. EMBO J 16:3822-3832.

Pellerin L, Bouzier-Sore AK, Aubert A, Serres S, Merle M, Costalat R, Magistretti PJ. 2007. Activity-dependent regulation of energy metabolism by astrocytes: an update. Glia 55:1251-1262.

Perry VH, Cunningham C, Boche D. 2002. Atypical inflammation in the central nervous system in prion disease. Curr Opin Neurol 15:349-354.

Perry VH, Hume DA, Gordon S. 1985. Immunohistochemical localization of macrophages and microglia in the adult and developing mouse brain. Neuroscience 15:313-326.

Pihlaja R, Koistinaho J, Malm T, Sikkila H, Vainio S, Koistinaho M. 2008. Transplanted astrocytes internalize deposited beta-amyloid peptides in a transgenic mouse model of Alzheimer's disease. Glia 56:154-163.

Platt FM WS. 2004. Lysosomal Disorders of the Brain. Oxford.

Ravikumar B, Berger Z, Vacher C, O'Kane CJ, Rubinsztein DC. 2006. Rapamycin pre-treatment protects against apoptosis. Hum Mol Genet 15:1209-1216.

Reichenbach A, Derouiche A, Kirchhoff F. 2010. Morphology and dynamics of perisynaptic glia. Brain Res Rev 63:11-25.

Ridet JL, Malhotra SK, Privat A, Gage FH. 1997. Reactive astrocytes: cellular and molecular cues to biological function. Trends Neurosci 20:570-577.

Roeser D, Preusser-Kunze A, Schmidt B, Gasow K, Wittmann JG, Dierks T, von Figura K, Rudolph MG. 2006. A general binding mechanism for all human sulfatases by the formylglycine-generating enzyme. Proc Natl Acad Sci U S A 103:81-86.

Rubinsztein DC. 2006. The roles of intracellular protein-degradation pathways in neurodegeneration. Nature 443:780-786.

Sardiello M, Annunziata I, Roma G, Ballabio A. 2005. Sulfatases and sulfatase modifying factors: an exclusive and promiscuous relationship. Hum Mol Genet 14:3203-3217.

Sattler R, Tymianski M. 2001. Molecular mechanisms of glutamate receptor-mediated excitotoxic neuronal cell death. Mol Neurobiol 24:107-129.

Schlotawa L, Ennemann EC, Radhakrishnan K, Schmidt B, Chakrapani A, Christen HJ, Moser H, Steinmann B, Dierks T, Gartner J. 2011. SUMF1 mutations affecting stability and activity of formylglycine generating enzyme predict clinical outcome in multiple sulfatase deficiency. Eur J Hum Genet 19:253-261.

Schmidt B, Selmer T, Ingendoh A, von Figura K. 1995. A novel amino acid modification in sulfatases that is defective in multiple sulfatase deficiency. Cell 82:271-278.

Settembre C, Annunziata I, Spampanato C, Zarcone D, Cobellis G, Nusco E, Zito E, Tacchetti C, Cosma MP, Ballabio A. 2007. Systemic inflammation and neurodegeneration in a mouse model of multiple sulfatase deficiency. Proc Natl Acad Sci U S A 104:4506-4511.

Settembre C, Arteaga-Solis E, McKee MD, de Pablo R, Al Awqati Q, Ballabio A, Karsenty G. 2008a. Proteoglycan desulfation determines the efficiency of

chondrocyte autophagy and the extent of FGF signaling during endochondral ossification. Genes Dev 22:2645-2650.

Settembre C, Fraldi A, Jahreiss L, Spampanato C, Venturi C, Medina D, de Pablo R, Tacchetti C, Rubinsztein DC, Ballabio A. 2008b. A block of autophagy in lysosomal storage disorders. Hum Mol Genet 17:119-129.

Sherwood CC, Stimpson CD, Raghanti MA, Wildman DE, Uddin M, Grossman LI, Goodman M, Redmond JC, Bonar CJ, Erwin JM, Hof PR. 2006. Evolution of increased glia-neuron ratios in the human frontal cortex. Proc Natl Acad Sci U S A 103:13606-13611.

Shih AY, Erb H, Sun X, Toda S, Kalivas PW, Murphy TH. 2006. Cystine/glutamate exchange modulates glutathione supply for neuroprotection from oxidative stress and cell proliferation. J Neurosci 26:10514-10523.

Sleat DE, Wiseman JA, El-Banna M, Kim KH, Mao Q, Price S, Macauley SL, Sidman RL, Shen MM, Zhao Q, Passini MA, Davidson BL, Stewart GR, Lobel P. 2004. A mouse model of classical late-infantile neuronal ceroid lipofuscinosis based on targeted disruption of the CLN2 gene results in a loss of tripeptidyl-peptidase I activity and progressive neurodegeneration. J Neurosci 24:9117-9126.

Sloane JA, Blitz D, Margolin Z, Vartanian T. 2010. A clear and present danger: endogenous ligands of Toll-like receptors. Neuromolecular Med 12:149-163.

Sofroniew MV. 2005. Reactive astrocytes in neural repair and protection. Neuroscientist 11:400-407.

Sokoloff L. 1999. Energetics of functional activation in neural tissues. Neurochem Res 24:321-329.

Staretz-Chacham O, Choi JH, Wakabayashi K, Lopez G, Sidransky E. 2010. Psychiatric and behavioral manifestations of lysosomal storage disorders. Am J Med Genet B Neuropsychiatr Genet 153B:1253-1265.

Tanaka K, Watase K, Manabe T, Yamada K, Watanabe M, Takahashi K, Iwama H, Nishikawa T, Ichihara N, Kikuchi T, Okuyama S, Kawashima N, Hori S, Takimoto M, Wada K. 1997. Epilepsy and exacerbation of brain injury in mice lacking the glutamate transporter GLT-1. Science 276:1699-1702.

Tansey MG, Goldberg MS. 2010. Neuroinflammation in Parkinson's disease: its role in neuronal death and implications for therapeutic intervention. Neurobiol Dis 37:510-518.

Tuppo EE, Arias HR. 2005. The role of inflammation in Alzheimer's disease. Int J Biochem Cell Biol 37:289-305.

Vaughn JE, Pease DC. 1967. Electron microscopy of classically stained astrocytes. J Comp Neurol 131:143-154.

Vaughn JE, Peters A. 1967. Electron microscopy of the early postnatal development of fibrous astrocytes. Am J Anat 121:131-152.

Vergarajauregui S, Connelly PS, Daniels MP, Puertollano R. 2008. Autophagic dysfunction in mucolipidosis type IV patients. Hum Mol Genet 17:2723-2737.

Von Figura K GV, Jaeken J. 2001. Metachromatic leukodystrophy. In: CR Scriver AB, WS Sly, D Valle, editor. The Metabolic and Molecular Basis of Inherited Disease. New York: McGraw-Hill. pp 3695–3724.

Wada R, Tifft CJ, Proia RL. 2000. Microglial activation precedes acute neurodegeneration in Sandhoff disease and is suppressed by bone marrow transplantation. Proc Natl Acad Sci U S A 97:10954-10959.

Weidemann A, Kerdiles YM, Knaup KX, Rafie CA, Boutin AT, Stockmann C, Takeda N, Scadeng M, Shih AY, Haase VH, Simon MC, Kleinfeld D, Johnson RS. 2009. The glial cell response is an essential component of hypoxia-induced erythropoiesis in mice. J Clin Invest 119:3373-3383.

Whitney ER, Kemper TL, Rosene DL, Bauman ML, Blatt GJ. 2008. Calbindin-D28k is a more reliable marker of human Purkinje cells than standard Nissl stains: a stereological experiment. J Neurosci Methods 168:42-47.

Wilson JX. 1997. Antioxidant defense of the brain: a role for astrocytes. Can J Physiol Pharmacol 75:1149-1163.

Wu YP, Matsuda J, Kubota A, Suzuki K. 2000. Infiltration of hematogenous lineage cells into the demyelinating central nervous system of twitcher mice. J Neuropathol Exp Neurol 59:628-639.

Yamanaka K, Chun SJ, Boillee S, Fujimori-Tonou N, Yamashita H, Gutmann DH, Takahashi R, Misawa H, Cleveland DW. 2008. Astrocytes as determinants of disease progression in inherited amyotrophic lateral sclerosis. Nat Neurosci 11:251-253.

Yu AC, Drejer J, Hertz L, Schousboe A. 1983. Pyruvate carboxylase activity in primary cultures of astrocytes and neurons. J Neurochem 41:1484-1487.

Yu L, McPhee CK, Zheng L, Mardones GA, Rong Y, Peng J, Mi N, Zhao Y, Liu Z, Wan F, Hailey DW, Oorschot V, Klumperman J, Baehrecke EH, Lenardo MJ. 2010. Termination of autophagy and reformation of lysosomes regulated by mTOR. Nature 465:942-946.

Yu T, Shakkottai VG, Chung C, Lieberman AP. 2011. Temporal and cell-specific deletion establishes that neuronal Npc1 deficiency is sufficient to mediate neurodegeneration. Hum Mol Genet 20:4440-4451.

Zatloukal K, Stumptner C, Fuchsbichler A, Heid H, Schnoelzer M, Kenner L, Kleinert R, Prinz M, Aguzzi A, Denk H. 2002. p62 Is a common component of cytoplasmic inclusions in protein aggregation diseases. Am J Pathol 160:255-263.

Acknowledgements